

# Projection scrubbing: a more effective, data-driven fMRI denoising method

Damon Pham<sup>1</sup>, Daniel McDonald<sup>2</sup>, Lei Ding<sup>1</sup>, Mary Beth Nebel<sup>3,4</sup>, and Amanda Mejia<sup>1</sup>

<sup>1</sup>Department of Statistics, Indiana University, Bloomington, IN, USA

<sup>2</sup>Department of Statistics, University of British Columbia, Vancouver, BC, Canada

<sup>3</sup>Center for Neurodevelopmental and Imaging Research, Kennedy Krieger Institute, Baltimore, MD, USA

<sup>4</sup>Department of Neurology, Johns Hopkins University, Baltimore, MD, USA

## Abstract

Functional MRI (fMRI) data are subject to artifacts arising from a myriad of sources, including subject head motion, respiration, heartbeat, scanner drift, and thermal noise. These artifacts cause deviations from common distributional assumptions, introduce spatial and temporal outliers, and reduce the signal-to-noise ratio of the data—all of which can have negative consequences on the accuracy and power of statistical analyses. Scrubbing is a technique for excluding fMRI volumes thought to be contaminated by artifacts. Motion scrubbing based on subject head motion derived measures, while popular, suffers from a number of drawbacks, among them the need to choose a threshold, high rates of scrubbing, consequent exclusion of subjects, and a lack of sensitivity to non-motion related artifacts. Data-driven scrubbing methods, which are instead based on observed noise in the processed fMRI timeseries, may avoid many of these issues and achieve higher sensitivity and specificity to artifacts. Here we present “projection scrubbing”, a new data-driven scrubbing method based on a statistical outlier detection framework. Projection scrubbing consists of two main steps: projection of the data onto directions likely to represent artifacts, and quantitative comparison of each volume’s association with artifactual directions to identify volumes exhibiting artifacts. Compared with DVARS, which is also data-driven, a primary advantage of projection scrubbing is its use of a common reference to identify abnormal volumes, rather than differences between subsequent volumes. We assess the ability of projection scrubbing to improve the reliability and predictiveness of functional connectivity (FC) compared with motion scrubbing and DVARS. We also compare projection methods, including independent component analysis (ICA), principal component analysis (PCA), and a novel fused PCA method. We perform scrubbing in conjunction with regression-based denoising through CompCor, which we found to outperform alternative methods. Projection scrubbing and DVARS were both substantially more beneficial to FC reliability than motion scrubbing, illustrating the advantage of data-driven measures over head motion-based measures for identifying contaminated volumes. ICA-based projection scrubbing produced the most

benefit to FC reliability overall. The benefit of scrubbing was strongest for connections between subcortical regions and cortical-subcortical connections. Scrubbing with any method did not have a noticeable effect on prediction accuracy of sex or total cognition, suggesting that the ultimate effect of scrubbing on downstream analysis depends on a number of factors specific to a given analysis. To promote the adoption of effective fMRI denoising techniques, all methods are implemented in a user-friendly, open-source R package that is compatible with NIFTI- and CIFTI-format data.

## 1 Introduction

Neuronal activity measured by the blood-oxygen-level dependent (BOLD) signal makes up only a small component of the total fluctuation in fMRI data (Lindquist, 2008; Bianciardi et al., 2009). A myriad of artifactual sources of variation cause fMRI data to exhibit low signal-to-noise ratio (SNR) and deviations from common distributional assumptions—e.g. Gaussianity, stationarity, homoskedasticity—due to artifacts’ spatiotemporal patterns and variable magnitude. Therefore, it is vital to remove as much noise from fMRI data as possible prior to statistical analysis. This is a difficult task, because the potential sources of noise are diverse in their origin and manifestation. For example, artifacts may be introduced due to subject head motion, physiological processes such as respiration, heartbeat, and blood flow fluctuation, thermal noise, magnetic field non-uniformities, scanner drift, and even prior data pre-processing steps (Bianciardi et al., 2009; Liu, 2016; Caballero-Gaudes and Reynolds, 2017).

While a single gold standard denoising pipeline for fMRI data has yet to be widely accepted, many methods for modeling, detecting and removing artifacts have been proposed. These methods can be loosely grouped into two categories: regression-based methods and “scrubbing” (also known as “censoring” or “spike regression”). Regression-based methods assume that artifactual fluctuations can be modelled using external or data-driven sources of information and linearly separated from the data. For example, it is well-known that head motion induces artifacts (Power et al., 2012; Van Dijk et al., 2012; Satterthwaite et al., 2012; Yan et al., 2013), so rigid body realignment parameters and their extensions (i.e. higher-order terms, their derivatives, or the lagged time-courses) are often regressed from the data to minimize noise coincident with motion (Friston et al., 1996). However, spatially variable spin-history effects introduced by motion are difficult to model and can persist after the application of such methods (Yancey et al., 2011). Similarly, BOLD fluctuations caused by respiration and heartbeat can be minimized by measuring the physiological cycles with a pulse oximeter or by estimating them if temporal resolution is high enough (Le and Hu, 1996; Power et al., 2017; Agrawal et al., 2020) or if phase information is available (Cheng and Li, 2010). An alternative approach to directly modeling sources of non-neural variability is to use tissue-based regressors from brain compartments thought to represent noise as a proxy for these sources, e.g., signals in the cerebrospinal fluid (CSF) and white matter (Behzadi et al., 2007; Muschelli et al., 2014; Caballero-Gaudes and Reynolds, 2017; Satterthwaite et al., 2019). Removal of the global

signal across the brain parenchyma remains a popular “catch-all” denoising technique due to its ability to remove noise for which more targeted techniques may lack sensitivity (Power et al., 2014; Ceric et al., 2017; Parkes et al., 2018b; Satterthwaite et al., 2019) but is controversial due to its potential to worsen existing artifacts, remove neurologically-relevant variation between subjects and induce anti-correlations (Liu et al., 2017; Power et al., 2017; Caballero-Gaudes and Reynolds, 2017; Parkes et al., 2018b). Finally, noise-related signals can be identified via independent component analysis (ICA) using ICA-FIX (Salimi-Khorshidi et al., 2014) or ICA-AROMA (Pruim et al., 2015) and regressed from the data.

Regression-based methods are effective at mitigating low- and medium-frequency nuisance signals, but they may be less powerful against “burst noise” caused by sudden head motion, irregular breaths, or hardware malfunction, which is difficult to model due to its unpredictable incidence and structure (Power et al., 2012; Yan et al., 2013; Parkes et al., 2018b; Satterthwaite et al., 2019). Therefore, another, complementary approach is to identify and remove volumes that are highly contaminated, a process known as *scrubbing*. The most popular scrubbing techniques are *motion scrubbing* based on frame-wise displacement (FD), a summary measure of head movement relative to the the previous volume (Power et al., 2012, 2014), and *DVARS*, a measure of the change in image intensity from the previous volume (Smyser et al., 2010; Power et al., 2012). Both motion scrubbing and DVARS require the choice of a threshold to identify volumes to remove. Afyouni and Nichols (2018) recently formulated DVARS as a sum-of-squares decomposition and proposed two DVARS-related measures that can be thresholded in a principled way. For motion scrubbing, however, there is no principled or universally accepted FD threshold above which volumes are considered contaminated. While a range of thresholds between 0.2 and 0.5 are commonly used in the literature (Power et al., 2014; Ceric et al., 2017; Afyouni and Nichols, 2018), the rate of scrubbing can vary dramatically across this range, and the downstream effects of different choices are not well-understood.

While motion scrubbing is arguably the most popular form of scrubbing used in fMRI analyses, it has a number of disadvantages in addition to the ambiguity of choosing a threshold. First, the percentage of volumes flagged for removal is often high, particularly for lower (more stringent) FD thresholds, which can result in unintentional removal of relevant signal. It is also common practice to exclude subjects for whom too many volumes are scrubbed, so over-aggressive removal of volumes can result in the exclusion of a substantial number of study participants. Second, recent work has shown that respiratory motion can artificially inflate head motion estimates and may result in the erroneous removal of volumes not concurrent with head motion (Fair et al., 2020). These artifacts in head motion estimates may be present in single-band fMRI data but are exacerbated using multi-band acquisitions (Gratton et al., 2020). Given the accelerating adoption of multi-band acquisitions and the growing availability of multi-band fMRI data through the Human Connectome Project (HCP) and other publicly available datasets adopting HCP-style acquisitions, e.g., the UK Biobank (Miller et al., 2016), the Developing Human Connectome Project (Hughes et al., 2017), the Adolescent Brain and Cognitive Development (ABCD)

study (?), and the Baby Connectome Project (Howell et al., 2019), the likelihood of over-aggressive removal presents a major concern for which there is currently no clear remedy. Furthermore, since the majority of studies comparing regression-based denoising and scrubbing techniques have focused on single-band fMRI acquisition (Ciric et al., 2017; Parkes et al., 2018b), the true effects of motion scrubbing in multi-band fMRI are largely understudied. Third, subject motion may induce artifacts that persist into subsequent time points. Power et al. (2012) and others have proposed flagging time points adjacent to high-FD volumes too, but this expansion applies to all high-FD volumes equally and thus may yield false positives. Finally, FD is computed prior to, and independent of, any denoising strategies, and therefore may flag volumes that actually exhibit low degrees of noise after regression-based noise reduction strategies have been applied.

In contrast to FD, data-driven scrubbing metrics can be computed after denoising in order to flag only those volumes that still exhibit high levels of contamination. Data-driven scrubbing techniques are also capable of identifying burst noise that is not due to subject head motion. Here we present a data-driven, statistically principled scrubbing approach known as *projection scrubbing*. This approach consists of two main steps. First, the data is *projected* onto directions likely to represent artifacts using strategic dimension reduction and selection. Second, each volume’s temporal activity associated with those directions is formally *compared* to the distribution across all volumes to identify statistical abnormalities or spikes representing burst noise (Mejia et al., 2017). By contrast, both FD and DVARS are based on comparing each volume to only its temporal predecessor. They are therefore also sensitive to repetition time (TR) (though it is now possible to properly normalize DVARS as proposed by Afyouni and Nichols (2018)). Projection scrubbing can be combined with robust outlier detection methods at the second step to enhance sensitivity and specificity in flagging volumes exhibiting statistical abnormalities (Mejia et al., 2017). We introduce two important improvements to the original projection scrubbing method proposed by Mejia et al. (2017). First, while the original framework used principal component analysis (PCA) for the projection step, we consider two alternative techniques that are more effective at identifying artifactual directions in the data: ICA and a novel technique, FusedPCA. Second, we propose a kurtosis-based selection method to separate and retain components of artifactual origin from those more likely to represent neuronal sources.

The goal of this work is two-fold: first, to assess the performance of projection scrubbing compared with popular scrubbing techniques; and second, to compare its performance using different projections (PCA, ICA, and FusedPCA) to determine the optimal method. In assessing the performance of each scrubbing method, it is important to recognize that noise reduction accompanied by drastic loss of meaningful signal, e.g. due to *over-scrubbing*, can be detrimental. Indeed, noise reduction strategies generally must achieve a balance between removal of noise and loss of true signal. We therefore assess the ability of scrubbing to maximize the presence of the neuronal signal, relative to the noise in the data, via two indirect measures of SNR in fMRI: the *reliability* and *predictiveness* of functional connectivity

(FC). For reliability, we specifically consider greater reliability to mean a higher proportion of variance attributable to unique subject-level features, i.e. more individualized FC. We quantify this using the intra-class correlation coefficient, as in a number of previous studies (e.g., Shehzad et al., 2009; Zuo et al., 2010; Thomason et al., 2011; Guo et al., 2012; Shirer et al., 2015), and fingerprinting match rate. This is an important distinction from other reliability metrics such as test-retest mean squared error (MSE) or correlation, which are effective at assessing noise reduction but do not penalize loss of subject-level signal. For example, setting FC to a constant value for all subjects would yield an MSE equal to zero, i.e. perfect reliability. For predictiveness, we consider the ability of FC to predict two measures: biological sex and total cognitive ability.

The remainder of this paper proceeds as follows. In Section 2, we describe the projection scrubbing framework, including our FusedPCA dimension reduction technique and novel kurtosis-based approach for selecting artifactual components. We also describe the reliability and prediction studies performed to compare projection scrubbing with existing scrubbing techniques. In Section 3, we report the performance of projection scrubbing, motion scrubbing and DVARS at improving the reliability and predictiveness of FC. Finally, we conclude with a discussion of our findings, limitations and future directions in Section 4.

## 2 Methods

### 2.1 Projection scrubbing

*Projection scrubbing* is the process of identifying and removing fMRI volumes exhibiting statistically unusual patterns likely to represent artifacts. The process of projection scrubbing involves projecting high-dimensional fMRI volumes onto a small number of directions likely to represent artifacts, then summarizing those directions into a single measure of deviation or outlyingness for each volume that can be thresholded to identify volumes contaminated with artifacts. This process consists of three steps, described in turn below: dimension reduction and selection of directions likely to represent artifacts, computing a measure of outlyingness for each volume, and thresholding that measure to identify artifactual volumes. All steps are implemented in the `fMRIscrub` R package.

#### 2.1.1 Dimension reduction and selection of artifactual directions

Let  $T$  be the duration of the fMRI timeseries, and let  $V$  be the number of brain locations included for analysis.  $\mathbf{Y}_{T \times V}$  is the vectorized fMRI BOLD timeseries, which has undergone basic preprocessing, typically including rigid body realignment to adjust for participant motion, spatial warping of the data to a standard space (e.g. distortion correction, co-registration to a high resolution anatomical image), and optional spatial smoothing. After robustly centering and scaling the timecourse of each brain location

(which can be voxels in volume space and/or vertices in surface space), we aim to project  $\mathbf{Y}$  to  $\mathbf{X}_{T \times Q}$ , which represents the timeseries associated with  $Q$  latent directions in the data. In Mejia et al. (2017), PCA was used for this purpose, and the top  $Q$  PCs explaining 50% of the data variance were retained. This choice was based on the observation that a source of severe burst noise (e.g. banding artifacts caused by head motion) will cause high-variance fluctuations, so its artifact pattern will tend to manifest in a high-variance PC. Here, we propose several improvements to this original framework to better distinguish directions representing artifactual variation from those representing neuronal variation: (1) the use of improved projection methods for better separation of artifactual directions in the data; (2) a principled method of dimensionality selection; and (3) a novel kurtosis-based method to identify components likely to represent artifacts. Each of these is described in turn below.

First, we consider two projection techniques to better to identify artifactual directions in the data compared with the original PCA approach: ICA and FusedPCA. ICA applied to fMRI typically aims to decompose the data into a set of maximally independent spatial components and a mixing matrix representing the temporal activity associated with each spatial component. The ability of ICA to separate fMRI data into spatial sources of neuronal and artifactual origin is well-established (McKeown et al., 1998). ICA has been used successfully for noise reduction in fMRI, most notably via ICA-FIX (Griffanti et al., 2014) and ICA-AROMA (Pruim et al., 2015).

*FusedPCA* is a novel PCA technique that employs a fusion penalty on the principal component time series. The fusion penalty has two effects: (1) it encourages a small number of larger jumps in the time series, which may make it easier to detect volumes contaminated with artifacts; and (2) it more easily finds sequential outliers, a common feature of fMRI artifacts. FusedPCA recognizes that volumes contaminated by artifacts, as well as those not contaminated by artifacts, tend to occur in sequential groups. Effectively, the PC scores for volumes in the same category (containing artifacts or free of artifacts) should be similar but differ dramatically from those in the other category. Thus, FusedPCA imposes a piecewise-constant constraint on the PC scores such that the scores for the artifactual volumes are more likely to occur sequentially and are much larger than the PC scores for the non-artifactual volumes. FusedPCA is a PCA version of constant trend filtering (Tibshirani, 2014; Kim et al., 2009) and is an instance of the penalized matrix decomposition framework presented in (Witten et al., 2009). The optimization problem defining FusedPCA and its estimation procedure are described in Appendix A.

Second, for all projection methods, we determine the number of components to estimate automatically using penalized semi-integrated likelihood (PESEL) (Sobczyk et al., 2017), a Bayesian probabilistic PCA approach that generalizes and improves upon the popular method of Minka (2000).

Finally, we propose a *novel* kurtosis-based method for selection of components likely to represent artifacts. Artifacts caused by burst noise tend to be both severe and transient. Therefore, a component (e.g. IC or PC) representing an artifactual spatial pattern will have associated timeseries (e.g. IC mixing or PC

scores) likely containing spikes or *outliers* at those time points where the artifact exists. The presence of these outliers alters the distribution of temporal activity associated with that component. In particular, *kurtosis*, the standardized fourth moment of a distribution, will be increased by the presence of these outliers. The kurtosis of a set of values,  $\mathbf{x} = (x_1, \dots, x_N)$  is computed as

$$\text{Kurt}(\mathbf{x}) = \sum_{i=1}^N \left( \frac{x_i - \bar{x}}{s} \right)^4 - 3,$$

where  $\bar{x}$  and  $s$  are respectively the sample mean and standard deviation of  $\mathbf{x}$ . The true kurtosis of Gaussian-distributed data is 0, but sample kurtosis will exhibit sampling variance. Sampling distributions of kurtosis for Gaussian-distributed data are shown in Appendix Figure B.1. We select those components whose timeseries have sample kurtosis significantly larger than what would be expected in Gaussian-distributed data, defined as exceeding the 0.99 quantile of the sampling distribution of kurtosis for a particular sample size. This corresponds to a probability of 0.01 for a false positive, i.e. falsely selecting an outlier-free component. As illustrated in Appendix Figure B.1, for time series of long duration (over  $T = 1000$ ), it is appropriate to use the theoretical asymptotic sampling distribution of kurtosis to determine the 0.99 quantile; for shorter time series, we use Monte Carlo simulation.

For kurtosis-based component selection, it is important that the data be detrended prior to projection or that the component timeseries be directly detrended. Appendix Figure B.2 illustrates the consequences of failing to detrend properly. Both mean and variance detrending of the component timeseries are implemented in the `fMRIscrub` R package. However for the analyses described below, we detrend the data prior to projection and therefore forego component detrending. Details of our data detrending procedure are given in Section 2.3.

### 2.1.2 Quantifying and thresholding outlyingness

Let  $\mathbf{X}_{T \times Q}$  contain the timeseries associated with the  $Q$  high-kurtosis components (PCs or ICs) after any detrending. Since the selected components are believed to represent artifacts, *outliers* or spikes in their associated timeseries can be used to locate the temporal occurrence of artifacts. We compute an aggregate (multivariate) measure of the temporal outlyingness of each volume, *leverage*, which can be used to identify spikes occurring across any of the components or in multiple components. Leverage is defined as the diagonal entries of the orthogonal projector onto the column space of  $\mathbf{X}$ ,  $\mathbf{H} = \mathbf{X}(\mathbf{X}^\top \mathbf{X})^{-1} \mathbf{X}^\top$ , and is related to Mahalanobis distance. In the linear regression context,  $\mathbf{H}$  is called the “hat matrix” and leverage is related to the influence of each observation on the coefficient estimates. In our context, leverage is an approximation of the influence of each volume on the selected components (Mejia et al., 2017). Since these components are selected because they are likely to represent artifacts, leverage can be interpreted as a *composite measure of the strength of artifactual signals* in each volume.

The final step is to threshold leverage to identify volumes contaminated by artifacts. To determine an

appropriate threshold, it is important to note that the total leverage over all  $T$  volumes is mathematically fixed at  $Q$ . Therefore, the high leverage associated with any outliers will decrease the leverage of all other volumes. Thus, the mean leverage will always be  $Q/T$ , but the leverage of a typical (non-outlying) volume may be much lower. Therefore, we use the median leverage across all volumes as a reference value, and consider volumes with leverage greater than a factor of the median to be outliers. Mejia et al. (2017) considered a range of thresholds between 3 and 8 times the median, and found 4 to be near optimal. Here, we consider a range of thresholds up to 8 times the median to provide updated evidence for an appropriate choice of threshold, given the improved methods, different evaluation metrics, and multi-band data being considered here.

## 2.2 Alternative scrubbing methods

For comparison, we consider the following alternative scrubbing methods: motion scrubbing using frame-wise displacement (FD) (Power et al., 2012, 2014) and DVARS (Smyser et al., 2010; Afyouni and Nichols, 2018). While FD is based on head motion and DVARS is based on BOLD signal change, both measure the change from the previous volume.

**Motion Scrubbing.** Head motion is estimated by assuming the brain is a rigid body and realigning all volumes to a chosen reference (e.g., the mean across all volumes). FD is calculated from the rigid body realignment parameters according to the formula  $FD(t) = |\Delta d_{xt}| + |\Delta d_{yt}| + |\Delta d_{zt}| + |\Delta \alpha_t| + |\Delta \beta_t| + |\Delta \gamma_t|$ , where  $\Delta q_t = q_t - q_{t-1}$  (Power et al., 2012). At volume  $t$ ,  $d_{xt}$ ,  $d_{yt}$  and  $d_{zt}$  represent the change in the brain’s estimated position along the  $x$ ,  $y$  and  $z$  coordinates, respectively relative to the reference, while  $\alpha_t$ ,  $\beta_t$  and  $\gamma_t$  represent the estimated rotation of the brain along the surface of a 50-mm-radius sphere (an approximation of the size of the cerebral cortex) relative to the same reference. Thus,  $FD(t)$  is equal to the sum of absolute changes in the realignment parameters (RPs, also known as the rigid body coordinates) between volume  $t$  and the previous frame. By convention  $FD(1) = 0$ . FD thresholds reported in the literature vary; thus, we consider a range of FD thresholds between 0.2 mm and 1.0 mm.

**DVARS Scrubbing.** Afyouni and Nichols (2018) propose two variations of DVARS, which can be thresholded in a principled manner: ZDVARS which measures statistical significance and  $\Delta\%DVARS$  which measures “practical” significance. Define  $A(t) = \frac{1}{V} \sum_{v=1}^V [\mathbf{Y}_{t,v}]^2$  and  $D(t) = \frac{1}{V} \sum_{v=1}^V [\frac{1}{2}(\mathbf{Y}_{t,v} - \mathbf{Y}_{t-1,v})]^2$ . Then the two variations are

$$ZDVARS(t) = \frac{D(t) - \text{median}(D)}{s_{hIQR}(D)} \quad \text{and} \quad \Delta\%DVARS(t) = \frac{D(t) - \text{median}(D)}{\text{mean}(A)} \times 100\%,$$

where  $s_{hIQR}$  estimates standard deviation robustly using the bottom half of the interquartile range (the first and second quartiles) and a power transformation ( $d = 3$  as selected by Afyouni and Nichols (2018)). ZDVARS represents a z-score for signal change, whereas  $\Delta\%DVARS$  measures the excess variance in the

signal change as a percentage of the mean signal change. Following Afyouni and Nichols (2018), we use an upper-tail 5% Bonferroni FWER significance level as the cutoff for ZDVARS, and 5% as the cutoff for  $\Delta\%$ DVARS. Only volumes exceeding both cutoffs are flagged by the “dual” DVARS cutoff method.

## 2.3 Data collection and processing

We analyze resting-state fMRI (rs-fMRI) from the Human Connectome Project (HCP) 1200-subject release and the HCP Retest Dataset (Van Essen et al., 2013). We use the minimally preprocessed (MPP) rs-fMRI data (Glasser et al., 2013) for our main analyses, but we include the rs-fMRI data denoised with ICA-FIX (Griffanti et al., 2014) for comparison. For the reliability study described in Section 2.4.1 below, we utilize the HCP test-retest data. Forty-five participants were enrolled in both the main and retest HCP studies, 42 of whom have both MPP and ICA-FIX versions of all rs-fMRI scans in full duration and are included in the analysis. Each test-retest subject has a total of eight runs collected across four visits (test session 1, test session 2, retest session 1, and retest session 2), using two acquisition sequences at each visit (LR and RL phase encoding). For the prediction study described in Section 2.4.2 below, we use the main HCP dataset, which includes 1,001 subjects with all four runs collected across two visits using the LR and RL acquisition sequences. Each rs-fMRI run includes 1200 volumes over a duration of approximately 15 minutes (TR = 0.72). The first 15 frames (just over 10 seconds) of each run are removed to account for magnetization stabilization. We analyze the data in “grayordinates” space resulting from the HCP surface processing pipeline of cortical data combined with the HCP volume processing pipeline for subcortical and cerebellar structures. This data consists of 91,282 gray matter brain locations across the left and right cortical surfaces, subcortical structures, and cerebellum.

### 2.3.1 Functional connectivity

In a series of analyses described below, we assess the impact of scrubbing on the reliability and predictiveness of FC. To compute FC, we calculate the average timeseries within each of 100 cortical regions defined by the Schaefer parcellation and within each of 19 Freesurfer parcels representing subcortical and cerebellar regions (**Figure 1**). The  $119 \times 119$  matrix of FC is computed as the Pearson correlation between each parcel timeseries. Prior to further analyses, a Fisher z-transformation is applied to map the FC values to the real line. Letting  $r$  represent Pearson correlation, the Fisher z-transformation is computed as  $z = \frac{1}{2} \ln \{(1 + r)/(1 - r)\}$ . We classify these 119 functional areas into seven cortical networks based on their overlap with the Yeo et al. (2011) seven-region parcellation and into five subcortical groupings based on location, function, and classical separation between midbrain and hindbrain structures.

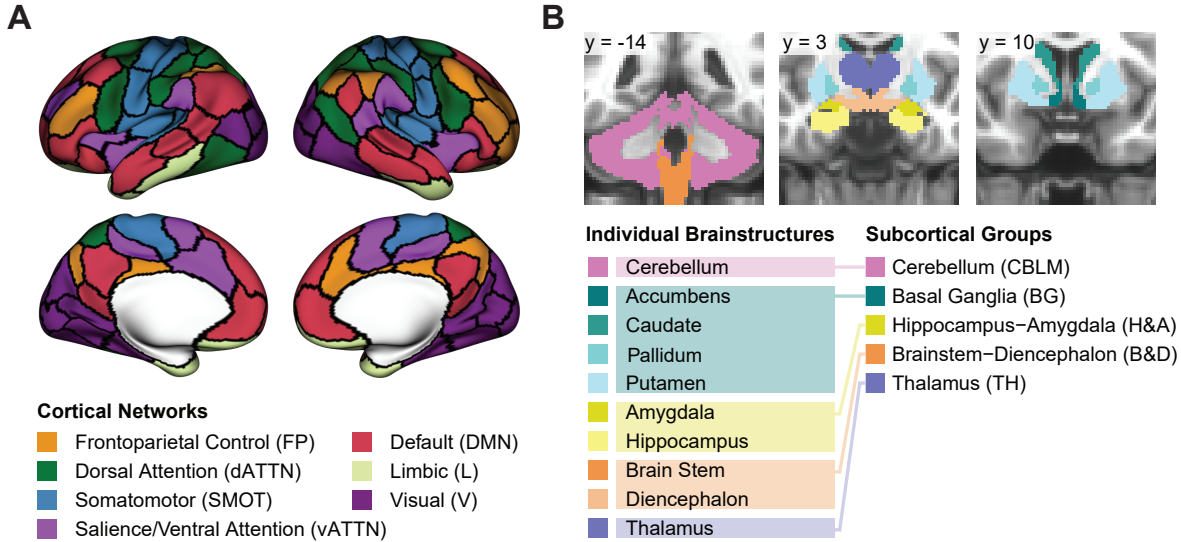


**Figure 1: Schaefer cortical parcellation and Freesurfer cerebellar and subcortical parcellation.** The 100 cortical parcels outlined in black and are grouped based on their overlap with the 7 Yeo networks (Yeo et al., 2011). Groupings of cerebellar and subcortical structures are indicated using color gradients. Note that all cerebellar and subcortical regions except the brainstem are separated into left and right hemisphere in our analysis.

### 2.3.2 Scrubbing and Denoising

**Figure 2** illustrates the data cleaning methods we employ in our comparative analysis of scrubbing techniques. All cleaning and scrubbing is performed in a simultaneous regression framework to avoid re-introducing artifacts through sequential processing (Lindquist et al., 2019). First, the original fMRI data is initially detrended and denoised, as described below. This attenuates trends and certain noise patterns, providing a lower noise floor and allowing for greater sensitivity of projection scrubbing and DVARS to burst noise. Second, spike regressors corresponding to volumes to be censored are added to the matrix of nuisance regressors. The original fMRI data are then simultaneously denoised and scrubbed using a single regression step.

**Data Denoising.** Long-lasting noise patterns (e.g. physiological cycles and scanner drift) cannot be efficiently mitigated by removing individual volumes alone. Regression-based denoising strategies are therefore complementary to scrubbing, since they remove noise components which last longer than a few frames. To determine the *marginal* benefit of scrubbing, we first obtain “baseline” FC estimates after regression-based denoising alone (indicated in blue in **Figure 2**). Then we estimate FC again based on the denoised and scrubbed data (indicated in green in **Figure 2**). The change in reliability or predictiveness of the FC estimates compared to the baseline yields the improvement attributable to a particular scrubbing method.

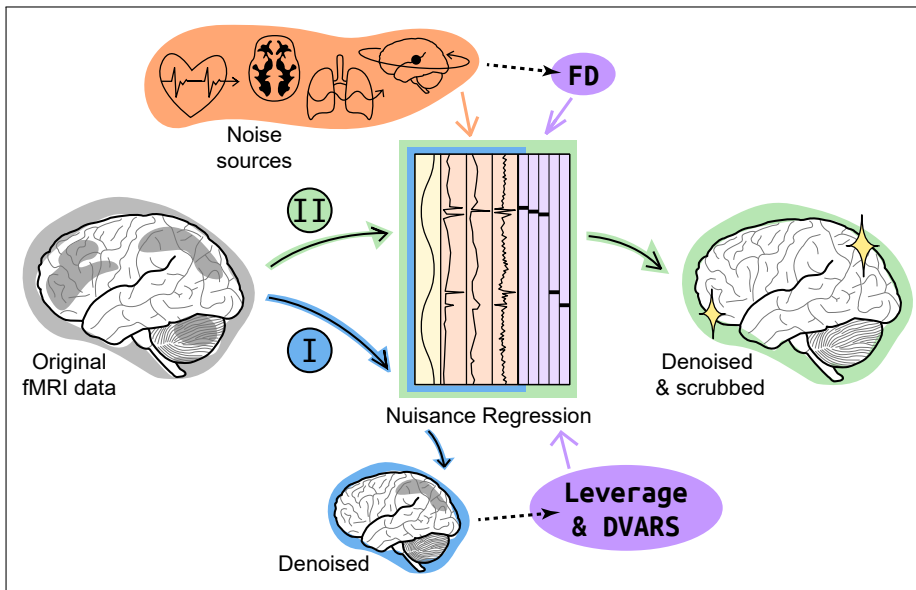


**Figure 2: Flowchart for fMRI data cleaning.** In our processing framework, fMRI data are denoised in a single simultaneous nuisance regression (blue) which removes shared variance with DCT bases (yellow) and noise components (orange). For projection scrubbing and DVARS (purple), volumes are flagged based on the denoised data, and nuisance regression is repeated (green) with a spike regressor for each flagged volume (purple) added to the design matrix. For motion scrubbing, since FD does not depend on the fMRI data, the denoised & scrubbed data can be computed directly without a preliminary nuisance regression.

Short Name	Description
MPP	No additional denoising
CC $x$	Anatomical CompCor based on the top $x \in \{1, \dots, 10\}$ principal components within masks of cerebral white matter, cerebral spinal fluid (CSF), and cerebellar white matter in volume space. Two voxel layers are eroded from the white matter ROIs, and one voxel layer is eroded from the CSF ROI.
2P	Mean signals from white matter (cerebral and cerebellar) and CSF. Erosion as in aCompCor.
9P	2P signals along with the six motion RPs and the global signal. Global signal is calculated across in-mask voxels in the volumetric MPP data.
36P	9P signals along with their one-back differences, squares, and squared one-back differences

**Table 1: Candidate denoising strategies.** All denoising strategies are applied to the minimally preprocessed (MPP) data via a regression framework using a design matrix including the noise regressors, an intercept, and (possibly) four DCT bases for detrending and high-pass filtering. The strategy resulting in the most reliable FC estimates will be adopted as the “baseline” denoising strategy, to be applied simultaneously with scrubbing.

Since the benefit of scrubbing depends on which denoising strategy is used, we first consider several options. The strategy yielding the most reliable FC estimates (highest mean ICC, see Section 2.4.1) will be adopted in subsequent analyses. We consider the following candidate strategies, described in Table 1: no additional denoising (minimal preprocessing, or MPP), anatomical CompCor (CC $x$ ), 2 parameter (P), 9P, and 36P (Behzadi et al., 2007; Satterthwaite et al., 2013a; Muschelli et al., 2014; Satterthwaite et al., 2019; Parkes et al., 2018b). For each denoising strategy, we also consider including four discrete cosine transform (DCT) bases for detrending and high-pass filtering. We adopt high-pass rather than band-pass filtering because removing high-frequency components from rs-fMRI has been shown to worsen signal-noise separation and reliability of FC estimates (Shirer et al., 2015).

We also include the HCP implementation of ICA-FIX for comparison. The volumetric and surface BOLD data and 24 motion parameters (6 RPs and their one-back differences, squares, and squared one-back differences) are all initially detrended with a nonlinear highpass filter. ICA is performed on the volumetric MPP BOLD data, and noise ICs are identified based on a trained classifier. The noise ICs are then “softly” regressed from the surface MPP BOLD data, along with 24 RPs, to avoid removing variance shared with the signal ICs (Griffanti et al., 2014).

**Scrubbing.** After determining a baseline denoising strategy, we add scrubbing to the regression-based

data cleaning, as illustrated in **Figure 2**. The baseline denoised data (blue) is used for computing DVARS and for identifying outlying volumes using projection scrubbing, i.e., projecting the data onto artifactual components and computing leverage for each volume. Volumes exceeding a specified threshold for leverage, DVARS or FD are flagged for removal. We consider a range of thresholds for projection scrubbing (2 to 8 times the median leverage, in multiples of 1) and FD (0.2 to 1.0 mm, in multiples of 0.1) and choose the one resulting in the most reliable estimates of functional connectivity (highest mean ICC, see Section 2.4.1).

We perform denoising and scrubbing in a simultaneous regression framework. A second, parallel nuisance regression on the original MPP data is performed using the same design matrix as in the baseline denoising, except with a spike regressor column added for each flagged volume (green path in **Figure 2**). Finally, flagged volumes are removed from the denoised and scrubbed data. Note that this is equivalent to censoring the flagged volumes in the MPP data and design matrix prior to the second nuisance regression.

It is important to note that the final data are obtained through a single simultaneous regression instead of multiple sequential regressions. This avoids the problem of latter regressors removing orthogonality between the cleaned data and prior regressors (Lindquist et al., 2019). For example, consider performing DCT detrending in one regression, followed by another regression with motion realignment parameters (RPs) estimated from the data prior to DCT detrending. The cleaned data will not necessarily be orthogonal to the DCT bases after the second regression, meaning that low-frequency trends might have been re-introduced to the data. Instead, if the DCT bases and RP regressors are combined in a single design matrix for a simultaneous regression, the cleaned data will be orthogonal to both the DCT bases and the RP regressors.

## 2.4 Methods comparison

To compare projection scrubbing with DVARS and motion scrubbing, we assess both the *reliability* and *predictiveness* of FC estimates based on the denoised and scrubbed data. Reliability is assessed using the intra-class correlation coefficient (ICC) (Shrout and Fleiss, 1979) and fingerprinting match rate. Predictiveness is based on the accuracy of predicting two demographic/behavioral measures from FC: *biological sex* and *total cognition*. The difference in reliability and predictiveness compared with baseline denoising yields the marginal improvement attributable to scrubbing.

### 2.4.1 Reliability study

When large amounts of data are available for individuals (as is the case for each HCP participant included in our analyses), patterns in FC have been shown to be primarily dominated by organizing principles

that are common across participants, as well as individual-specific elements of brain networks that are stable across time (Gratton et al., 2018). Effective noise-reduction strategies will therefore produce FC estimates that are more stable or reliable across multiple sessions collected from the same subject. Our metric of reliability, the ICC, can be thought of as a measure of how well an estimate reflects unique traits in a group of subjects.

To assess the test-retest reliability of FC estimates for each data cleaning strategy, we compute the ICC(3,1) of the Fisher z-transformed FC values. The ICC(3,1) is based on the relationship between mean sum-of-squares between (MSB) and mean sum-of-squares within (MSW). For a given data cleaning strategy and pair of brain regions, let  $z_{ij}$  represent the FC estimate for scan  $j = 1, \dots, J$  of subject  $i = 1, \dots, N$ , let  $M_i = \frac{1}{J} \sum_{j=1}^J z_{ij}$ , and let  $\bar{M} = \frac{1}{JN} \sum_{j=1}^J \sum_{i=1}^N z_{ij}$ . Then the ICC(3,1) is given by

$$\text{ICC}(3,1) = \frac{\text{MSB} - \text{MSW}}{\text{MSB} + (J-1)\text{MSW}},$$

where

$$\text{MSB} = \frac{J}{N-1} \sum_{i=1}^N (M_i - \bar{M})^2, \quad \text{and} \quad \text{MSW} = \frac{1}{N(J-1)} \sum_{i=1}^N \left( \sum_{j=1}^J (z_{ij} - M_i)^2 \right).$$

ICC represents a ratio of variances, with  $\text{ICC} = 1$  indicating that all of the variance in the estimates is attributable to between-subject differences, with no variance across repeated measures of the same individual. At the other extreme,  $\text{ICC} = 0$  indicates that all of the variance is attributable to within-subject variance across repeated measures, with no variance in the underlying measure across subjects. We adopt ICC(3,1) rather than other ICC measures because it is appropriate for measuring test-retest reliability when the reliability of a single measurement is of interest (Koo and Li, 2016) and to facilitate comparison with previous studies of FC reliability (Caceres et al., 2009; Parkes et al., 2018b).

Since previous work has shown FC of individual subjects to be identifiable across multiple sessions (Finn et al., 2015), we conduct a fingerprinting analysis to assess the extent to which enhanced reliability leads to enhanced identifiability. That is, does scrubbing improve the fingerprinting match rate? We divide the eight scans available from each participant into four sets of runs paired by phase encoding acquisition and visit: the two test LR scans, the two test RL scans, the two retest LR scans, and the two retest RL scans. For each set of paired runs, fingerprinting is performed using the first scans as the database set and the second as the target/query set. For each scan in the query set, we calculate Pearson correlations between its FC and that of each scan in the database set. If the database scan with the highest correlation is from the same subject, the fingerprint is a match. This procedure is repeated swapping the roles of database set and query set within each pair to yield eight rounds of matching. The overall match rate is computed as the rate of successful matches across  $8 \times 42$  total queries. Since previous studies have shown that using connections only within a certain network can yield more accurate fingerprinting identifications than using all connections across the brain (Finn et al., 2015), we repeat this procedure using only the

connections involving each network or the subcortex.

#### 2.4.2 Brain-behavior prediction study

Scientifically useful estimates of FC are those that are not only more reliable, but also more reflective of demographic and cognitive characteristics of individuals (Finn and Rosenberg, 2021). If subjects' characteristics can be better predicted using the FC values resulting from a particular data cleaning method, that method can be thought to better reduce sources of noise, while preserving relevant neuronal signals, and hence being more predictive of individual characteristics. We predict two demographic variables available from the HCP: *biological sex* ("Gender") and *total cognition* ("CogTotalComp\_AgeAdj"). We chose sex because cognitive function is known to differ between males and females, and there is great interest in studying the neural basis of these differences (Satterthwaite et al., 2015; Dhamala et al., 2020). Additionally, many neurobiological disorders impact males and females differently, for instance autism (Jack et al., 2021; Hernandez et al., 2020), attention deficit hyperactivity disorder (Rosch et al., 2018), and chronic pain (Fauchon et al., 2021). Thus, reliable methods for investigating sex differences in functional connectivity are needed to delineate the pathophysiology of these conditions. The NIH Cognition Total Composite Score (referred to as "total cognition" in the HCP behavioral database) (Gershon et al., 2013; Weintraub et al., 2013) was chosen because data quality has been shown to impact the power of inter-individual variability in FC to predict inter-individual variability in cognitive performance (Siegel et al., 2017).

For this analysis, we exclude 18 subjects with fewer than 5 minutes of data remaining after scrubbing using any method for at least one run, or who had high levels of head motion (FD over 0.3) in at least half of their volumes across all four runs. We then balance the remaining 983 subjects for sex and motion within each age group (22 – 25, 26 – 30, 31 – 35 and over 36 years old) by randomly sampling subjects so that the median FD across males and females is as equal as possible within each age group. The balanced dataset includes  $n = 804$  (402 female) subjects. For the total cognition prediction model, we excluded 10 subjects without total cognition scores. Age-adjusted total cognition scores of the remaining 794 subjects range from 88.95 to 153.36, with a mean of 123.36 and a median of 121.58.

For both sex and total cognition, we use a regression framework with a variable selection penalty. For *sex* prediction, we use an elastic net penalty that encourages coefficient shrinkage as well as variable selection (Zou and Hastie, 2005; Friedman et al., 2010). The elastic net is a convex combination of LASSO (Tibshirani, 1996) and ridge penalties (Hoerl and Kennard, 1970) and usually combines strength from both for superior predictive accuracy. For *total cognition* prediction, we use ridge regression, since empirically we observe virtually no sparsity in the coefficients. For prediction of *sex* we use a logistic regression model; for prediction of *total cognition* we use a linear regression model with Gaussian errors. We predict total cognition separately for males and females, since the neurobiological correlates of

intelligence have been shown to vary in both pattern and strength by sex (Jiang et al., 2020a,b; Dhamala et al., 2021). We employ a nested cross-validation (CV) procedure to obtain out-of-sample predictions for each subject and session. The predictions are compared to the true values using standard measures of error: deviance (or log-loss) for *sex* and MSE for *total cognition*. Details of the cross-validation procedure are given in Appendix C. For obtain a set of coefficient values for each method, we re-estimate the model using all subjects and sessions.

## 3 Results

### 3.1 Selection of baseline denoising strategy and scrubbing thresholds

**Figure 3** displays the effect of different baseline denoising strategies on the strength and reliability of FC. **Figure 3A** displays average FC estimates across all subjects and sessions. Here we display just four of the denoising strategies for the sake of space: ICA-FIX, as it is provided by the HCP and is a popular ICA-based denoising method; minimal preprocessing (MPP), since all regression-based denoising is applied on top of the MPP data; CompCor2 (CC2) since it exhibited the best performance overall, as described below; and 36P since it illustrates the effect of including global signal regression. Both CC2 and 36P include detrending with 4 DCT bases. We observe two primary trends: first, we see clear differences in FC strength across methods, with CC2 having stronger connections than MPP or ICA-FIX, and 36P inducing off-diagonal negative FC values (e.g., between regions belonging to different functional networks) due to the inclusion of the global signal (Murphy et al., 2009). The strengthening of FC with CC2 relative to MPP is likely due to an improvement in signal-to-noise. The effect can be seen across the entire matrix of FC but is particularly noticeable for connections involving subcortical regions. Second, a checkerboard pattern of FC can be seen within network pairs (within the diagonal and off-diagonal blocks), particularly for the MPP data, suggesting differences in FC strength for intra- and inter-hemispheric connections. This pattern is attenuated or removed by CC2, explored further in panel (D).

**Figure 3B** examines the effect of different denoising strategies on the reliability of FC, in terms of the mean ICC across all connections. First, we observe that DCT4 detrending is nearly uniformly beneficial for reliability. It tends to yield greater improvement when combined with less effective denoising strategies. This may reflect differences across strategies in the level of implicit detrending they perform. For example, the MPP and 2P denoising show dramatic improvements to reliability with DCT4, suggesting that these methods may not achieve effective detrending on their own. From this point forward, DCT4 is assumed to be included in the data cleaning framework unless stated otherwise. The most reliable FC estimates are produced with low-order aCompCor denoising, with CC2 having the highest mean ICC. We also consider two extensions of CC2 to assess whether including motion parameters in addition to

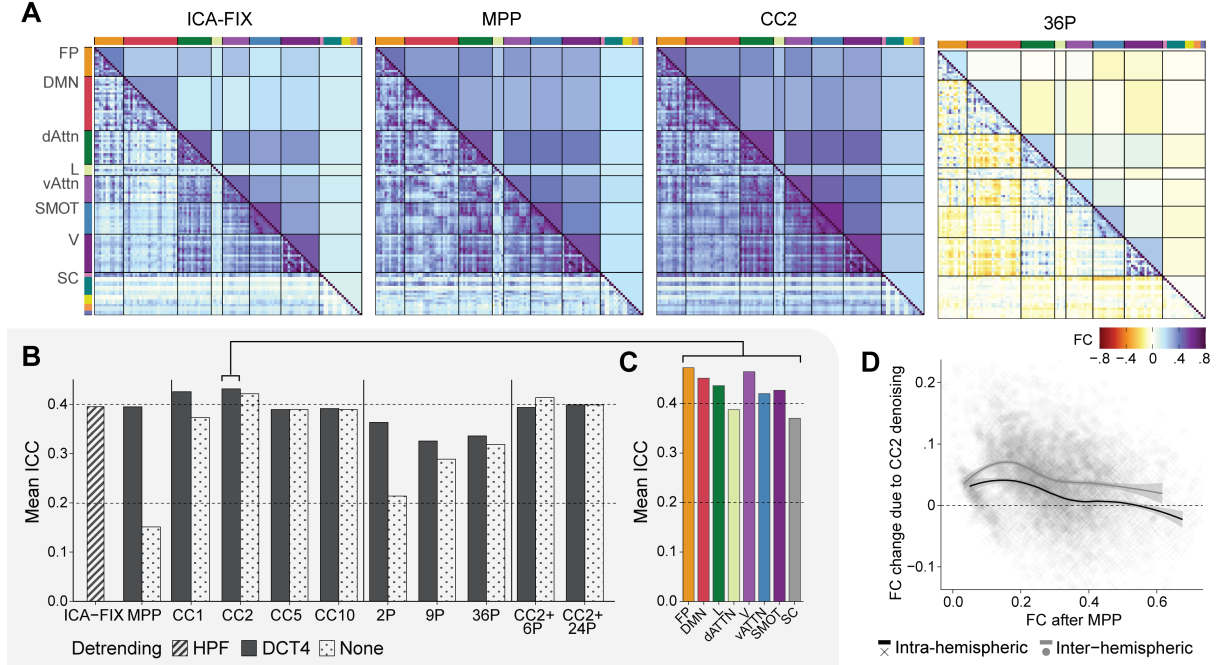


**Figure 3: Effects of different denoising methods on the strength and reliability of functional connectivity.** (A) Average FC estimates across subjects and sessions for different denoising strategies, from left to right: ICA-FIX, minimally preprocessed (MPP), CompCor with two components (CC2), and the 36 parameter model (36P). CC2 and 36P include detrending with four discrete cosine transform bases (DCT4). The rows and columns of each matrix represent the 119 regions, which are grouped primarily by network with subcortical regions last, and secondarily by hemisphere (left then right) (see Figure 1 for the subcortical legend). The upper triangle of each matrix displays average FC values for each network pair. (B) Effect of denoising on reliability of FC, in terms of the mean ICC across all connections. Based on these results, CC2 + DCT4 is adopted as the baseline denoising strategy in subsequent analyses. (C) Average reliability of connections involving each network after baseline denoising (CC2 + DCT4). (D) Effect of baseline denoising (CC2 + DCT4) on FC strength for inter- and intra-hemispheric cortical and subcortical connections. Each point represents a pair of parcels, and lines represent lowess smoothers with standard errors. Weaker connections and inter-hemispheric connections tend to be strengthened more by denoising.

white matter and CSF-derived signals results in more reliable FC. Specifically, we consider the inclusion of 6 RPs (CC2+6P) or those parameters along with their one-back differences, squares, and squared one-back differences (CC2+24P). In both cases, we observe worsened reliability compared with CC2 without motion parameters. Thus, we adopt CC2 as the baseline denoising strategy for all subsequent analyses.

**Figure 3C** displays the average reliability of connections involving each network after denoising with CC2. This shows that there are baseline differences in reliability prior to scrubbing, with the most reliable connections being those involving the fronto-parietal, attention and default mode networks, and the least reliable connections involving the limbic network and subcortical/cerebellar regions. **Figure 3D** explores the effect of denoising with CC2 on FC strength for intra- and inter-hemispheric cortical and subcortical connections. Two effects are clearly apparent. First, weak connections (below 0.3) tend to be strengthened the most by denoising. Second, inter-hemispheric connections are strengthened more than intra-hemispheric connections. This explains the near-elimination of the checkerboard pattern observed in the MPP matrix in **Figure 3A**. Thus, denoising may help to alleviate noise-related attenuation of long-range connections.

**Figure 4** examines the effect of different thresholds for FD and leverage on both the reliability of FC and on the proportion of volumes removed. For DVARS, we adopt the dual cutoff as described in (Afifi and Nichols, 2018), which results in mean ICC improvement of 0.0057 and removal of 2.5% of frames on average. For FD, the most reliable FC estimates are produced using a threshold of 0.3 mm, which results in removal of approximately 10% volumes on average. We therefore adopt this value, which is between the “lenient” (0.5 mm) “stringent” (0.2 mm) cutoffs characterized by (Power et al., 2014) and is in the neighborhood of values often adopted in the literature.

For projection scrubbing, we consider all three projection methods (ICA, PCA and FusedPCA) described above. While they exhibit similar reliability and removal rates, the highest overall reliability is achieved with ICA and FusedPCA at a threshold of 3 times the median. Note that similar reliability is achieved with a threshold of 4 times the median, which was recommended by Mejia et al. (2017). We therefore adopt a cutoff of 3, which results in approximately 3–4% of volumes being removed on average, depending on the projection. Notably, projection scrubbing removes *fewer than half* the number of volumes than motion scrubbing, yet achieves *more than double* the improvement to reliability. Compared with DVARS, projection scrubbing removes slightly more volumes but results in more overall improvement to reliability. Projection scrubbing will be compared in more detail with DVARS and motion scrubbing in subsequent analysis, but these high-level findings suggest that it tends to produce the most reliable FC estimates overall. From this point forward, we consider only the ICA and FusedPCA projection methods, since they tend to outperform the original PCA-based approach.

It is important to ensure that sufficient data remains for each scan (Ciric et al., 2017; Parkes et al.,

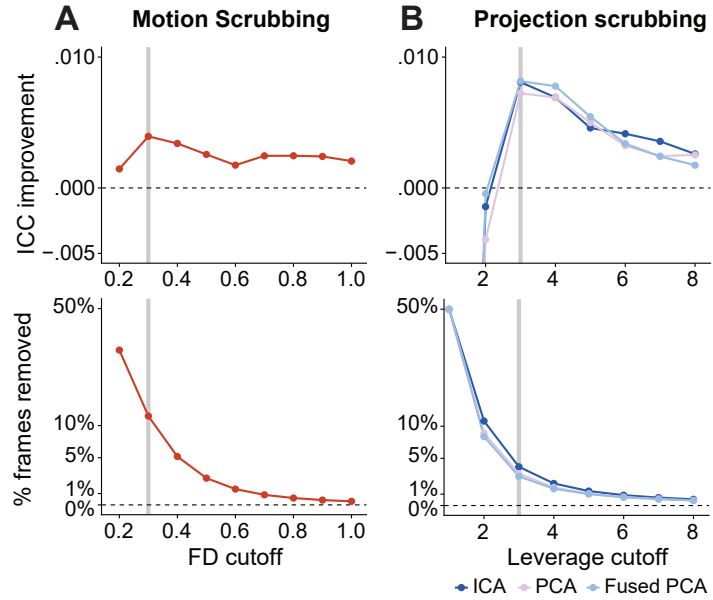


**Figure 4: Selection of scrubbing thresholds.** **(A)** We consider FD cutoffs between 0.2 and 1.0 mm in multiples of 0.1 mm. A threshold of 0.3 mm (indicated by the vertical gray line) results in the greatest improvement to FC reliability. At this threshold, approximately 10% of volumes are scrubbed on average. **(B)** For projection scrubbing, we consider leverage cutoffs between 2 and 8 times the median, in multiples of 1. A threshold of 3-times the median (indicated by the vertical gray line) results in the greatest improvement to FC reliability for all three projection methods (ICA, FusedPCA and PCA). At this threshold, 3 – 4% of volumes are scrubbed on average, depending on the projection. Notably, leverage scrubbing censors fewer than half the number of volumes as motion scrubbing, while producing more than double the improvement to overall reliability.

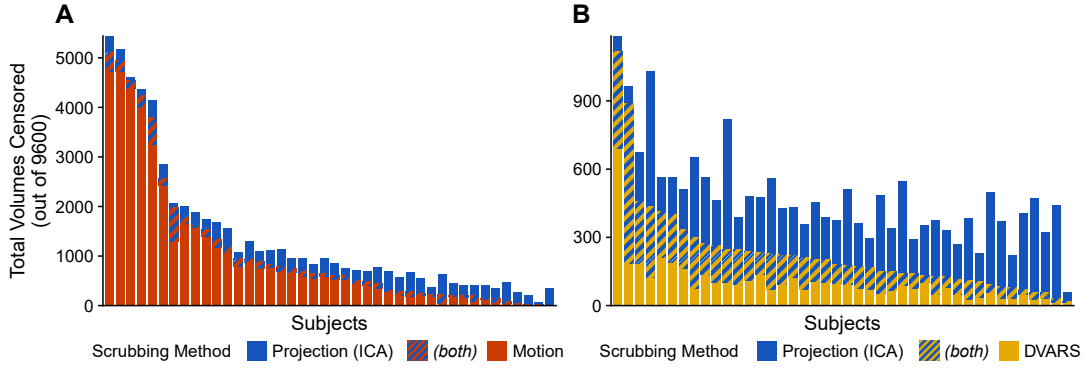


**Figure 5: Overlap between ICA projection scrubbing and other scrubbing methods. (A)** The number of volumes flagged per subject by motion scrubbing, projection scrubbing, or both. Motion scrubbing tends to flag a much larger number of volumes compared with projection scrubbing. The overlap between volumes flagged with projection scrubbing versus motion scrubbing is fairly small. Similar patterns of overlap with motion scrubbing are seen for DVARS and FusedPCA projection scrubbing (results not shown). **(B)** The number of volumes flagged per subject by DVARS, projection scrubbing, or both. The overlap between DVARS and projection scrubbing is moderate, though a substantial number of volumes are flagged by only one but not both methods.

2018a). For projection scrubbing and DVARS, all scans had at least 900 volumes (75%, or 10 minutes) remaining after scrubbing. For FD, only three of 336 total scans had fewer than 5 minutes remaining after scrubbing, and all scans retained at least 350 volumes (30%, or 4.2 minutes). Thus, we did not omit any scans from our study on the basis of excessive scrubbing.

Figure 5 examines the overlap between volumes flagged with projection scrubbing and those flagged with motion scrubbing and DVARS. We only consider ICA projection scrubbing here for brevity, but FusedPCA projection scrubbing shows similar patterns of overlap. There is strikingly little overlap between projection scrubbing and motion scrubbing, shown in **Figure 5A**. Motion scrubbing typically flags a much higher number of volumes. Using projection scrubbing, only a small portion of high-FD volumes are typically flagged, and a majority of the volumes flagged are not associated with high levels of head motion. Patterns of overlap with motion scrubbing are similar for DVARS (results not shown). This suggests two fundamental differences between motion scrubbing and data-driven scrubbing such as DVARS and projection scrubbing: first, many volumes with high FD do not exhibit abnormal patterns of intensity after denoising; second, many volumes without high FD exhibit abnormalities, likely due to other sources of artifacts.

Considering the overlap between projection scrubbing and DVARS shown in **Figure 5B**, the two methods often flag a large number of common volumes. However, for most subjects there is a substantial portion of volumes identified by only one technique, showing that the two methods work in different ways and

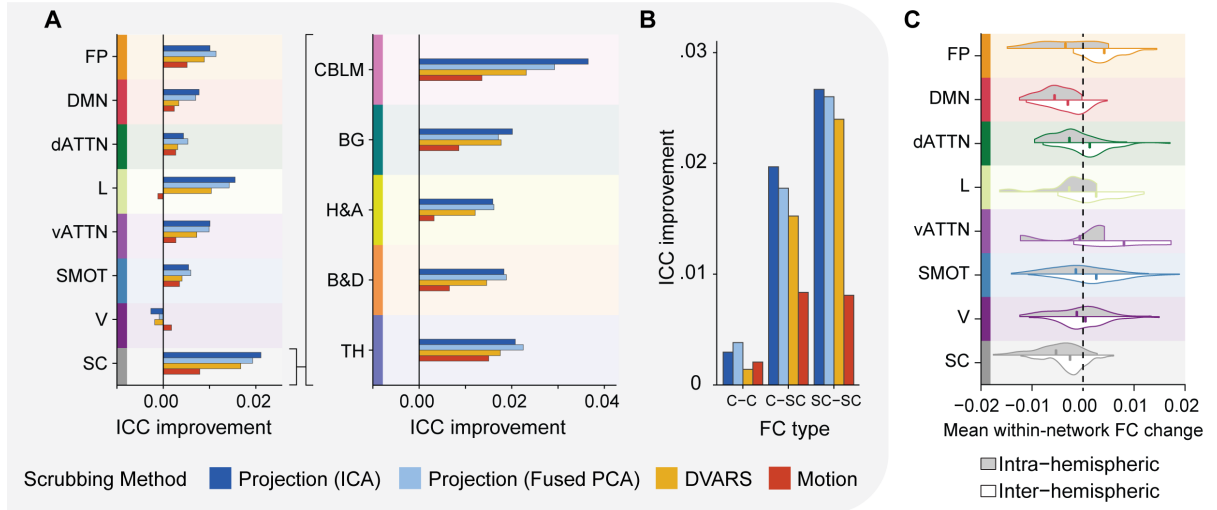


**Figure 6: Effect of scrubbing on FC reliability and strength.** (A) The average change in ICC (over baseline CC2 denoising) across all connections involving a given network or subcortical group. Projection scrubbing produces greater improvement to FC reliability than DVARS or motion scrubbing across nearly all networks and subcortical groups. (B) Effect of scrubbing on reliability of FC for cortical-cortical (C-C) connections, cortical-subcortical (C-SC) connections, and subcortical-subcortical (SC-SC) connections. Connections involving subcortical regions (SC-SC and C-SC) tend to enjoy the greatest improvement in reliability due to scrubbing. (C) Effect of ICA-based projection scrubbing on FC strength. Split violin plots display the distribution of change in FC strength due to scrubbing for all within-network intra- and inter-hemispheric connections. Vertical bars within each violin half indicate the mean value. On average, scrubbing increases the strength of inter-hemispheric FC relative to intra-hemispheric FC.

produce different results, even though they have fairly similar rates of scrubbing, and similar effects on overall reliability of FC as described below.

### 3.2 Reliability study results

**Figure 6** displays the effects of different scrubbing methods on the reliability of FC, relative to baseline denoising with CC2. **Figure 6A** shows the average change in ICC across all connections involving a particular network. Generally, scrubbing tends to improve reliability of FC for nearly all networks. Second, projection scrubbing with ICA or FusedPCA tends to improve reliability of FC the most, followed by DVARS, with motion scrubbing showing the worst performance across all networks with the exception of the visual network, which is affected negligibly by scrubbing in general. Third, scrubbing results in the most dramatic improvements in FC reliability for connections involving cerebellar and subcortical areas. Strong improvements are also observed for connections involving the limbic, ventral attention, and fronto-

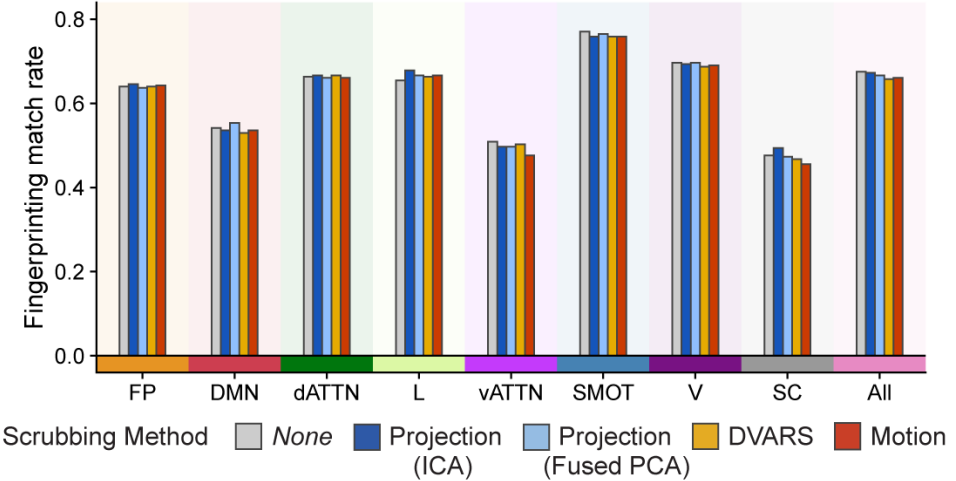


**Figure 7: Fingerprinting match rate for different brain regions.** Fingerprinting was performed using all connections or only the connections involving a certain network.

parietal networks. Finally, projection scrubbing with ICA or FusedPCA exhibit similar performance, but ICA results in substantially higher reliability for connections involving the cerebellum.

**Figure 6B** shows the effect of scrubbing on FC reliability by cortical and subcortical involvement. For all types of connections, data-driven scrubbing (projection scrubbing and DVARS) is more beneficial to FC reliability than motion scrubbing. The strongest improvement in reliability from scrubbing is to subcortical-subcortical connections, closely followed by cortical-subcortical connections. For these connections, ICA projection scrubbing results in the greatest improvement to FC reliability. Cortical-cortical connections also improve overall, but to a much smaller degree. Appendix D shows similar plots for other baseline denoising methods. Data-driven scrubbing is nearly universally beneficial, though the magnitude of benefit varies by denoising method. Data-driven scrubbing methods consistently produce more benefit to FC reliability than motion scrubbing, and projection scrubbing tends to perform slightly better than DVARS.

**Figure 6C** shows the effect of ICA projection scrubbing on the strength of within-network FC. Vertical bars within each split violin plot indicate the mean value. On average, inter-hemispheric connections tend to be strengthened relative to intra-hemispheric connections due to scrubbing. This mimics a similar effect of regression-based denoising with CC2 (see Figure 3D). However, scrubbing tends to *decrease* FC strength of intra-hemispheric within-network connections. Other scrubbing methods show a similar effect (results not shown). This suggests that scrubbing may reduce inflated FC of short-range connections due to artifacts, as well as potentially also alleviating attenuation of longer-range connections (Satterthwaite et al., 2013b).

**Figure 7** shows the fingerprint match rate for each scrubbing method. There is virtually no change in fingerprinting success due to scrubbing. This is likely because the benefits of scrubbing are not

dramatic enough to systematically affect which subjects are matched to each other. The highest match rate is achieved using connections involving the motor and visual networks. The match rate using all connections is greater than 60%, which is similar to using only connections involving the dorsal attention, frontoparietal, or limbic networks. These success rates are all much greater than the success rate of random guesses (1 in 42, or less than 3%).

### 3.3 Brain-behavior prediction study results

For the prediction study, we only consider the ICA version of projection scrubbing, since it shows better performance than FusedPCA in terms of reliability. **Figure 8** shows results of the models predicting *sex* and *total cognition* based on functional connectivity. **Figure 8A** displays estimated regression coefficients for each prediction model. Recall that FC values are generally positive after denoising with CC2, as shown in **Figure 3**. Therefore, positive coefficients indicate that stronger connectivity is associated with higher predicted values, while negative coefficients indicate that stronger connectivity is associated with lower predicted values. For the model for *sex*, larger values correspond to increased probability of being male. The coefficients for sex prediction are quite sparse, with a mix of negative and positive values within most network pairs. Stronger connections within the frontoparietal and dorsal attention networks are associated with being male, while stronger connections within the ventral attention and motor networks are associated with being female. Connections between the motor network and the ventral attention and frontoparietal networks are also associated with being male. For prediction of *total cognition*, the patterns and strength of coefficients are distinct across males and females. Most strikingly, the coefficients for females are larger in magnitude overall, which is consistent with the lower CV prediction error for females versus males. This suggests that there is a stronger association between FC and total cognition scores for females. For the female model, stronger connections within the visual network, and between the visual network and the ventral attention and limbic networks, are associated with higher cognition scores.

**Figure 8B** displays the cross-validation (CV) error using each scrubbing method, with the null model error indicated by the dashed line. The CV error plot for *sex* shows that FC-based prediction of sex is quite successful, with all models showing substantially lower error than the null model. The CV error plot for *total cognition* shows that FC only predicts total cognition slightly better than guessing for both sexes, with the female model being somewhat more predictive. For both the sex and total cognition models, scrubbing using any method does not appear to significantly change overall prediction error.

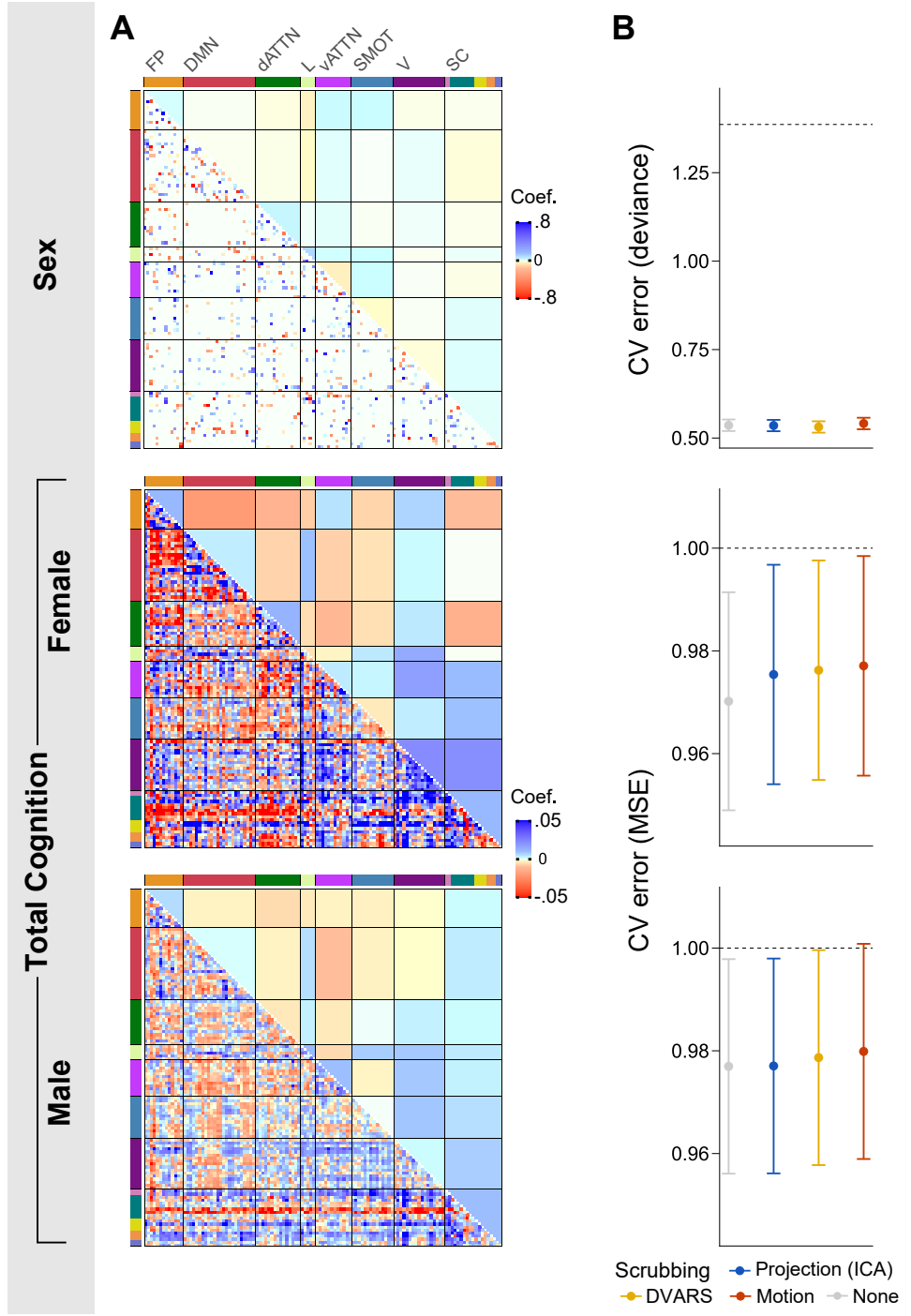


**Figure 8: Results of prediction models for sex and total cognition.** (A) Model coefficient estimates for each prediction model. Estimates are based on no scrubbing, since estimates after scrubbing appear very similar (results not shown). The upper triangle of each matrix displays the average coefficient value within each network-pair. Positive coefficients (blue) indicate that stronger connectivity is associated with *higher* predicted values, while negative coefficients (red) indicate that stronger connectivity is associated with *lower* values. For sex prediction, predicted values correspond to the probability of being male. (B) Cross-validation (CV) error for models based on FC estimates obtained after scrubbing with each method. Lower values indicate more accurate predictions. The dashed line indicates the null model error, equivalent to guessing.

## 4 Discussion

Here, we have presented projection scrubbing, a data-driven, statistically principled method of identifying and removing fMRI volumes contaminated by artifacts. We consider two projection methods for identifying artifactual directions in the projection scrubbing framework: ICA and a novel FusedPCA method. We compare the performance of projection scrubbing with motion scrubbing and DVARS at producing reliable and predictive subject-level estimates of functional connectivity. Our results show that projection scrubbing produces more reliable FC estimates than motion scrubbing or DVARS, with ICA projection resulting in the best performance overall. Below, we discuss these results in more detail, describe some potential reasons for the effectiveness of projection scrubbing, and note some considerations for scrubbing more generally.

### 4.1 Projection scrubbing is less aggressive and more effective than motion scrubbing

One of the most striking findings in our analysis is that projection scrubbing tends to result in much stronger improvement to FC reliability compared with traditional motion scrubbing, while removing around half the number of volumes. On average, motion scrubbing removes approximately 10% of the volumes in each scan, while ICA projection scrubbing removes fewer than half that amount. Examining the overlap with motion scrubbing, we observe that ICA projection scrubbing tends to identify only a small proportion of high-FD volumes. Indeed, in our analyses most volumes flagged via projection scrubbing are typically not coincident with head motion. This suggests two phenomena: first, many motion-related artifacts may be alleviated through regression-based denoising and therefore do not manifest as burst noise in the denoised data; second, projection scrubbing identifies a significant amount of burst noise likely caused by other sources, such as scanner artifacts, spillover effects of previous head motion, or artifacts introduced through preprocessing. This suggests that projection scrubbing’s greater gains in FC reliability are due to being both more *specific* (avoiding unnecessary removal of clean volumes) and more *sensitive* (identifying a wider range of artifacts) compared with motion scrubbing.

Despite the less aggressive rate of removal, the improvement to FC reliability with projection scrubbing is substantially greater than motion scrubbing for many connections, particularly for those involving the fronto-parietal, DMN, limbic and ventral attention networks. For connections involving subcortical regions (including cortical-subcortical connections), projection scrubbing exhibits 2-3 times greater benefit than motion scrubbing overall. Notably, the only connections for which motion scrubbing outperforms any other method were those involving the visual network, which were only affected negligibly by scrubbing in general.

The less aggressive but more effective censoring achieved by projection scrubbing has significant implica-

tions for data retention in fMRI studies. Because even submillimeter head movements have been shown to impact functional connectivity (Power et al., 2012; Van Dijk et al., 2012; Satterthwaite et al., 2012), it is common for researchers to eliminate entire scans from an analysis based on FD restrictions (see Ceric et al. (2017) and Parkes et al. (2018b) for examples). This practice can lead to drastic reductions in sample size. For instance, in a study examining the impact of motion artifact denoising procedures on predictions of brain maturity from rs-fMRI data, Nielsen et al. (2019) began by excluding 365 of 487 participants between 6 and 35 years of age due to excessive head motion. Similarly, Marek et al. (2019) excluded 40% of ABCD participants despite efforts to track head motion in real-time to ensure a sufficient amount of motion-free data would be collected from each participant (Casey et al., 2018). Data-driven scrubbing methods, i.e. projection scrubbing and DVARS, provide more targeted removal of contaminated volumes, which would allow for more data retention and help to increase the number of subjects ultimately included in analysis of fMRI studies.

## 4.2 Projection scrubbing improves upon DVARS by going beyond differences

Both leverage and DVARS are data-driven metrics, and as such have two main advantages over motion scrubbing: first, they can identify artifacts not related to motion (higher sensitivity); second, they can avoid flagging volumes that have been effectively cleaned via regression-based denoising (higher specificity), hence retaining more meaningful signal and ultimately improving SNR. While both projection scrubbing and DVARS result in substantially more improvement to FC reliability than motion scrubbing in our analyses, projection scrubbing consistently results in more improvement than DVARS. Specifically, ICA projection scrubbing achieves greater improvement in reliability across all cortical networks and subcortical regions than DVARS, with the most substantial differences seen for connections involving the DMN, limbic and ventral attention networks and cerebellar regions. A fundamental distinction between DVARS and projection scrubbing is that DVARS is computed based on the *difference* between each volume and the previous volume, while projection scrubbing uses leverage, a measure of outlyingness describing each volume's *deviation from the distribution* across all volumes. Projection scrubbing therefore incorporates information from all volumes in quantifying the abnormality of individual volumes, and as a result may be more accurate at identifying temporal abnormalities. For example, if volume  $t - 1$  is contaminated with artifact but volume  $t$  is not, the latter may be erroneously censored with DVARS but not with projection scrubbing. A second distinction is that projection scrubbing is based on first extracting directions (e.g., independent components) in the data that are likely to represent artifactual patterns. This may also have the effect of making leverage more sensitive and specific to artifacts.

### 4.3 Relationship of ICA projection scrubbing to ICA-based denoising

Considering the various dimension reduction techniques considered for projection scrubbing, ICA shows the most benefit to FC reliability in our analyses. This approach builds upon established methods employing ICA to identify and remove artifacts in fMRI data, most notably ICA-FIX (Salimi-Khorshidi et al., 2014) and ICA-AROMA (Pruim et al., 2015). Like those approaches, ICA projection scrubbing takes advantage of the ability of ICA to separate neuronal sources from those of artifactual origin in fMRI. However, ICA projection scrubbing has several clear differences from ICA-based denoising methods. We will focus on comparing with ICA-FIX since it is more general than ICA-AROMA, which is primarily focused on removing motion-related artifacts. First, as a scrubbing technique, ICA projection scrubbing is not designed for general denoising, unlike ICA-FIX. However, it can be effectively combined with established regression-based denoising techniques, such as CompCor or motion regression, as illustrated here. Second, the classification problem faced in the context of ICA projection scrubbing is simpler than that of ICA-FIX, since we assume the data has been partially denoised using regression-based methods prior to performing ICA. Therefore, the artifactual ICs being classified by ICA-FIX are likely to exhibit a wider range of temporal properties than those being classified in the ICA projection scrubbing framework. This is reflected by the fact that the classifier used in ICA-FIX is based on over 180 spatial and temporal features, while ICA projection scrubbing is based on a single temporal metric, kurtosis, that is indicative of the temporal spikes or bursts characteristic of artifactual sources. Third, ICA projection scrubbing is fully automated, while ICA-FIX is based on a trained classifier that requires manual IC labelling for high accuracy. Projection scrubbing instead employs a formal hypothesis testing approach to identify those ICs with high kurtosis, avoiding the need for model training. A limitation of this study is that we have not directly examined the accuracy of this approach at separating signal and noise ICs. This would be a useful area of future work. However, we note that perfect IC classification is not necessary in the projection scrubbing framework, since all noise ICs are pooled to identify volumes exhibiting temporal abnormalities representing burst noise. Thus, errors in classification of a small number of individual ICs do not necessarily lead to errors in classification of volumes.

### 4.4 Scrubbing is a trade-off between noise removal and signal retention

An interesting finding in our analyses is that, while the reliability of connections involving cerebellar and subcortical regions improves dramatically with scrubbing, the reliability of connections involving visual regions actually tends to worsen slightly. This illustrates an important property of scrubbing: the potential to inadvertently discard meaningful signal along with the noise. The optimal balance between noise removal and signal retention in a given situation depends on the SNR properties of the underlying data, which may differ dramatically depending on acquisition and processing factors and varies markedly across the connectome. Certain connections enjoying high baseline SNR may benefit more from greater

signal retention than from more aggressive noise removal. Therefore, the amount of scrubbing, and whether scrubbing is warranted at all, should depend on the scientific goals and properties of the data. For example, multi-band acquisitions allow for higher temporal resolution, but at the cost of spatially variable noise amplification (Risk et al., 2021). In areas where this noise amplification is low (e.g., the visual and motor cortex), the benefits outweigh the costs in terms of the power to detect fMRI signal changes (Chen et al., 2015; Todd et al., 2017; Risk et al., 2018), but in cerebellar and subcortical regions noise amplification can be moderate to high respectively (Risk et al., 2021), and scrubbing is likely to be highly beneficial—as we have indeed observed. In contexts where the data is expected to exhibit high SNR, on the other hand, a more cautious and measured approach to scrubbing may be warranted.

The effect of scrubbing is also heavily dependent on the choice of baseline denoising technique. Generally, more effective regression-based denoising results in cleaner data containing less noise that needs to be removed through scrubbing. Indeed, previous studies have noted that scrubbing may be unnecessary or even detrimental when applied in addition to effective regression-based denoising, including CompCor and ICA-FIX (Muschelli et al., 2014; Cho et al., 2021). In our analysis, the choice of baseline denoising method was determined based on which method produced the most reliable FC prior to scrubbing, and therefore effectively minimized the noise remaining in the data to be addressed via scrubbing. Indeed, the magnitude of improvement to reliability we observe due to scrubbing is much smaller than that due to baseline denoising. This may also explain why scrubbing had virtually no effect on the fingerprinting match rate, because the small gains achieved by scrubbing on top of effective regression-based denoising are likely too subtle to cause systematic differences in matching.

#### 4.5 Benefit of scrubbing on downstream analysis depends on several factors

While our analyses showed that scrubbing consistently improved the reliability of FC, scrubbing with any method had no statistically significant effect on the success rate of FC-based fingerprinting or prediction of sex or total cognition. We posit that the benefit of scrubbing in a particular analysis relating FC to another measure of interest (e.g. subject identity, sex) depends on three main factors: the strength of the association with FC, the number of connections involved in that association, and whether the quantity being estimated is coarse or fine. In the case of total cognition prediction, FC appeared to be only weakly associated with the measure of interest, and thus scrubbing had little effect on predictive accuracy. In the case of sex prediction, FC appeared to be strongly associated with sex but only a few connections are involved in that association; thus, scrubbing only had a small benefit on predictive accuracy. Finally, in the case of fingerprinting, the FC-based measure of interest is the ranking of matches within and between subjects, a relatively coarse estimand; thus, small changes in the accuracy of FC are unlikely to “move the needle”. Therefore, while our reliability analyses suggest that projection scrubbing and data-driven scrubbing in general serve to improve the overall SNR of fMRI data, the practical benefit

of scrubbing depends largely on many details of the specific analysis being performed. Generally, our results suggest that data-driven scrubbing is more likely to be beneficial when *fine* or *precise* quantities are being estimated, which are *strongly* related to FC, and in which the *entire* connectome is involved. Two such examples are (1) prediction models where there is a strong relationship between FC and the outcome measure and where there is little sparsity in the coefficients and (2) continuous network metrics involving the full connectome. It is worth noting that scrubbing was not observed to be detrimental in any of our downstream analyses, and therefore could be incorporated into standard denoising pipelines with little risk of doing harm.

## 4.6 Limitations and Future Directions

There are several limitations of the projection scrubbing framework proposed here. First, the metric we employ, leverage, is related to Mahalanobis distance, a commonly used multivariate distance metric. It is not robust and could therefore be influenced by outliers. This can lead to what is known as *masking*, wherein truly outlying observations appear to fall within the normal range in the multivariate distribution, due to the influence of larger outliers on the parameters underlying a non-robust distance metric (Rousseeuw and Van Zomeren, 1990). The use of a robust distance measure in place of leverage is therefore an important future direction and could ultimately improve the sensitivity and specificity of projection scrubbing at identifying artifactual volumes. Second, here we employ an ad-hoc threshold for leverage. While our analysis, considered alongside the earlier findings of Mejia et al. (2017), shows that a threshold of 3 – 4 times the median leverage is a reasonable and likely near-optimal choice, a more principled threshold with controllable statistical properties is desirable. Mejia et al. (2017) considered a robust distance metric with a known theoretical null distribution (Hardin and Rocke, 2005), which could in theory be used to determine an appropriate threshold for identifying outlying volumes. However, the assumptions underlying the theory are restrictive and unlikely to hold in the case of fMRI data. Further work is needed to determine the null distribution of robust distance metrics for data that deviate from common assumptions such as Gaussianity and independence.

In this work, we compared projection scrubbing with popular existing scrubbing techniques. However, an alternative to scrubbing is imputation of the data or of signal IC timeseries using “despike” methods (Allen et al., 2011), such as 3dDespike from AFNI (Analysis of Functional Neuroimages: <http://afni.nimh.nih.gov>; NIMH Scientific and Statistical Computing Core, Bethesda, Maryland) or Wavelet Despike (Patel et al., 2014). Since these methods target the timeseries of specific brain locations or components, they are less heavy-handed than scrubbing, which targets entire volumes. They may therefore be able to retain more signal while reducing the effects of burst noise. A comparison of data-driven scrubbing and despiking methods would be a worthwhile direction of future research.

A further limitation of this study is that we have not directly examined the efficacy of our approach at

identifying artifactual directions in the data. Our method employs a single temporal metric, kurtosis, to select ICs (or other types of components) representing artifactual directions. We contend that this greatly simplified approach to identification of artifactual ICs, relative to ICA-FIX, is possible because the data has already been largely denoised through regression-based methods such as aCompCor. The overall strong performance of ICA projection scrubbing suggests that this approach is sufficiently accurate to form the basis for an effective data-driven scrubbing technique. However, it would be useful to formally assess and potentially refine the ability of this kurtosis-based approach to identify artifactual ICs.

Finally, further work may consider alternative projection methods as the basis for projection scrubbing. Here we considered ICA, FusedPCA and PCA in conjunction with a subsequent kurtosis cutoff to identify directions likely to represent artifacts. These projections attempt to estimate components that exhibit certain properties, e.g. independence in the case of ICA; however, what is of greater relevance in projection scrubbing is that the components represent patterns of burst noise in the data. Other projection or rotation methods may be better suited to this task, including methods that are designed to maximize kurtosis, such as projection pursuit (Hou and Wentzell, 2011) and varimax rotation (Rohe and Zeng, 2020), or dimension reduction methods designed specifically for the purpose of outlier detection (Kandanaarachchi and Hyndman, 2021).

## 5 Conclusion

In this paper, we propose a novel data-driven, statistically principled scrubbing technique known as *projection scrubbing*. We perform a thorough analysis of the effects of projection scrubbing on the reliability and predictiveness of functional connectivity, compared with motion scrubbing and DVARS. Our analyses show that data-driven scrubbing techniques tend to be much more beneficial than motion scrubbing, while retaining a substantially greater number of volumes. Compared with existing scrubbing techniques, projection scrubbing tends to produce more reliable estimates of functional connectivity.

## Acknowledgements

This work was supported in part by National Institute of Biomedical Imaging and Bioengineering (NIBIB) grant R01EB027119 to A.F.M. and M.B.N.; National Science Foundation (NSF) CAREER grant DMS-1753171 and the National Sciences and Engineering Research Council of Canada (NSERC) grant RGPIN-2021-02618 to D.J.M.; and National Institute of Mental Health (NIMH) grant K01MH109766 to M.B.N.

## References

Afyouni, S. and Nichols, T. E. (2018). Insight and inference for DVARS. *NeuroImage*, 172:291–312.

Agrawal, U., Brown, E. N., and Lewis, L. D. (2020). Model-based physiological noise removal in fast fMRI. *NeuroImage*, 205:116231.

Allen, E. A., Erhardt, E. B., Damaraju, E., Gruner, W., Segall, J. M., Silva, R. F., Havlicek, M., Rachakonda, S., Fries, J., Kalyanam, R., et al. (2011). A baseline for the multivariate comparison of resting-state networks. *Frontiers in systems neuroscience*, 5:2.

Behzadi, Y., Restom, K., Liau, J., and Liu, T. T. (2007). A component based noise correction method (CompCor) for BOLD and perfusion based fMRI. *NeuroImage*, 37(1):90–101.

Bianciardi, M., Fukunaga, M., van Gelderen, P., Horovitz, S. G., de Zwart, J. A., Shmueli, K., and Duyn, J. H. (2009). Sources of functional magnetic resonance imaging signal fluctuations in the human brain at rest: a 7 T study. *Magnetic Resonance Imaging*, 27(8):1019–1029.

Caballero-Gaudes, C. and Reynolds, R. C. (2017). Methods for cleaning the BOLD fMRI signal. *NeuroImage*, 154:128–149.

Caceres, A., Hall, D. L., Zelaya, F. O., Williams, S. C. R., and Mehta, M. A. (2009). Measuring fMRI reliability with the intra-class correlation coefficient. *NeuroImage*, 45(3):758–768.

Casey, B., Cannonier, T., Conley, M. I., Cohen, A. O., Barch, D. M., Heitzeg, M. M., Soules, M. E., Teslovich, T., Dellarco, D. V., Garavan, H., et al. (2018). The adolescent brain cognitive development (abcd) study: imaging acquisition across 21 sites. *Developmental cognitive neuroscience*, 32:43–54.

Chen, L., Vu, A. T., Xu, J., Moeller, S., Ugurbil, K., Yacoub, E., and Feinberg, D. A. (2015). Evaluation of highly accelerated simultaneous multi-slice epi for fmri. *Neuroimage*, 104:452–459.

Cheng, H. and Li, Y. (2010). Respiratory noise correction using phase information. *Magnetic resonance imaging*, 28(4):574–582.

Cho, J. W., Korchmaros, A., Vogelstein, J. T., Milham, M. P., and Xu, T. (2021). Impact of concatenating fMRI data on reliability for functional connectomics. *NeuroImage*, 226:117549.

Ciric, R., Wolf, D. H., Power, J. D., Roalf, D. R., Baum, G. L., Ruparel, K., Shinohara, R. T., Elliott, M. A., Eickhoff, S. B., Davatzikos, C., Gur, R. C., Gur, R. E., Bassett, D. S., and Satterthwaite, T. D. (2017). Benchmarking of participant-level confound regression strategies for the control of motion artifact in studies of functional connectivity. *NeuroImage*, 154:174–187.

Dhamala, E., Jamison, K. W., Jaywant, A., and Kuceyeski, A. (2021). Shared functional connections within and between cortical networks predict individual cognitive abilities in males and females. *bioRxiv*.

Dhamala, E., Jamison, K. W., Sabuncu, M. R., and Kuceyeski, A. (2020). Sex classification using long-range temporal dependence of resting-state functional MRI time series. *Human Brain Mapping*, 41(13):3567–3579.

Fair, D. A., Miranda-Dominguez, O., Snyder, A. Z., Perrone, A., Earl, E. A., Van, A. N., Koller, J. M., Feczko, E., Tisdall, M. D., van der Kouwe, A., et al. (2020). Correction of respiratory artifacts in mri head motion estimates. *Neuroimage*, 208:116400.

Fauchon, C., Meunier, D., Rogachov, A., Hemington, K. S., Cheng, J. C., Bosma, R. L., Osborne, N. R., Kim, J. A., Hung, P. S. P., Inman, R. D., and Davis, K. D. (2021). Sex differences in brain modular organization in chronic pain. *Pain*, 162(4).

Finn, E. S. and Rosenberg, M. D. (2021). Beyond fingerprinting: Choosing predictive connectomes over reliable connectomes. *NeuroImage*, page 118254.

Finn, E. S., Shen, X., Scheinost, D., Rosenberg, M. D., Huang, J., Chun, M. M., Papademetris, X., and Constable, R. T. (2015). Functional connectome fingerprinting: identifying individuals using patterns of brain connectivity. *Nature Neuroscience*, 18(11):1664–1671.

Fisher, R. A. (1930). The moments of the distribution for normal samples of measures of departure from normality. *Proceedings of the Royal Society of London. Series A, Containing Papers of a Mathematical and Physical Character*, 130(812):16–28.

Friedman, J., Hastie, T., and Tibshirani, R. (2010). Regularization paths for generalized linear models via coordinate descent. *Journal of Statistical Software*, 33(1):1–22.

Friston, K. J., Williams, S., Howard, R., Frackowiak, R. S., and Turner, R. (1996). Movement-related effects in fMRI time-series. *Magnetic Resonance in Medicine*, 35(3):346–355.

Gershon, R. C., Wagster, M. V., Hendrie, H. C., Fox, N. A., Cook, K. F., and Nowinski, C. J. (2013). NIH toolbox for assessment of neurological and behavioral function. *Neurology*, 80(11 Suppl 3).

Glasser, M. F., Sotropoulos, S. N., Wilson, J. A., Coalson, T. S., Fischl, B., Andersson, J. L., Xu, J., Jbabdi, S., Webster, M., Polimeni, J. R., Van Essen, D. C., and Jenkinson, M. (2013). The minimal preprocessing pipelines for the Human Connectome Project. *NeuroImage*, 80:105–124.

Gratton, C., Dworetzky, A., Coalson, R. S., Adeyemo, B., Laumann, T. O., Wig, G. S., Kong, T. S., Gratton, G., Fabiani, M., Barch, D. M., et al. (2020). Removal of high frequency contamination from motion estimates in single-band fmri saves data without biasing functional connectivity. *NeuroImage*, 217:116866.

Gratton, C., Laumann, T. O., Nielsen, A. N., Greene, D. J., Gordon, E. M., Gilmore, A. W., Nelson, S. M., Coalson, R. S., Snyder, A. Z., Schlaggar, B. L., Dosenbach, N. U., and Petersen, S. E. (2018).

Functional Brain Networks Are Dominated by Stable Group and Individual Factors, Not Cognitive or Daily Variation. *Neuron*, 98(2).

Griffanti, L., Salimi-Khorshidi, G., Beckmann, C. F., Auerbach, E. J., Douaud, G., Sexton, C. E., Zsoldos, E., Ebmeier, K. P., Filippini, N., Mackay, C. E., Moeller, S., Xu, J., Yacoub, E., Baselli, G., Ugurbil, K., Miller, K. L., and Smith, S. M. (2014). ICA-based artefact removal and accelerated fMRI acquisition for improved resting state network imaging. *NeuroImage*, 95:232–247.

Guo, C. C., Kurth, F., Zhou, J., Mayer, E. A., Eickhoff, S. B., Kramer, J. H., and Seeley, W. W. (2012). One-year test–retest reliability of intrinsic connectivity network fmri in older adults. *Neuroimage*, 61(4):1471–1483.

Hardin, J. and Rocke, D. M. (2005). The distribution of robust distances. *Journal of Computational and Graphical Statistics*, 14(4):928–946.

Hernandez, L. M., Lawrence, K. E., Padgaonkar, N. T., Inada, M., Hoekstra, J. N., Lowe, J. K., Eilbott, J., Jack, A., Aylward, E., Gaab, N., Van Horn, J. D., Bernier, R. A., McPartland, J. C., Webb, S. J., Pelphrey, K. A., Green, S. A., Geschwind, D. H., Bookheimer, S. Y., and Dapretto, M. (2020). Imaging-genetics of sex differences in ASD: distinct effects of OXTR variants on brain connectivity. *Translational Psychiatry*, 10(1).

Hoerl, A. E. and Kennard, R. W. (1970). Ridge regression: Biased estimation for nonorthogonal problems. *Technometrics*, 12(1):55–67.

Hou, S. and Wentzell, P. (2011). Fast and simple methods for the optimization of kurtosis used as a projection pursuit index. *Analytica chimica acta*, 704(1-2):1–15.

Howell, B. R., Styner, M. A., Gao, W., Yap, P.-T., Wang, L., Baluyot, K., Yacoub, E., Chen, G., Potts, T., Salzwedel, A., et al. (2019). The unc/umn baby connectome project (bcp): An overview of the study design and protocol development. *NeuroImage*, 185:891–905.

Hughes, E. J., Winchman, T., Padorno, F., Teixeira, R., Wurie, J., Sharma, M., Fox, M., Hutter, J., Cordero-Grande, L., Price, A. N., et al. (2017). A dedicated neonatal brain imaging system. *Magnetic resonance in medicine*, 78(2):794–804.

Jack, A., Sullivan, C. A. W., Aylward, E., Bookheimer, S. Y., Dapretto, M., Gaab, N., Van Horn, J. D., Eilbott, J., Jacokes, Z., Torgerson, C. M., Bernier, R. A., Geschwind, D. H., McPartland, J. C., Nelson, C. A., Webb, S. J., Pelphrey, K. A., Gupta, A. R., Bernier, R. A., McPartland, J. C., Ventola, P., Kresse, A., Neuhaus, E., Corrigan, S., Wolf, J., McDonald, N., Ankenman, K., Webb, S. J., Jeste, S., Nelson, C. A., Naples, A., Libsack, E., Pelphrey, K. A., Aylward, E., Bookheimer, S. Y., Gaab, N., Dapretto, M., Van Horn, J. D., Jack, A., Guilford, D., Torgerson, C., Welker, O., Geschwind, D. H., Gupta, A. R., Sullivan, C. A. W., Lowe, J. K., Jacokes, Z., MacDonnell, E., Tsapelas, H.,

Depedro-Mercier, D., Keifer, C. M., and Ventola, P. (2021). A neurogenetic analysis of female autism. *Brain*.

Jiang, R., Calhoun, V. D., Cui, Y., Qi, S., Zhuo, C., Li, J., Jung, R., Yang, J., Du, Y., Jiang, T., et al. (2020a). Multimodal data revealed different neurobiological correlates of intelligence between males and females. *Brain imaging and behavior*, 14(5):1979–1993.

Jiang, R., Calhoun, V. D., Fan, L., Zuo, N., Jung, R., Qi, S., Lin, D., Li, J., Zhuo, C., Song, M., et al. (2020b). Gender differences in connectome-based predictions of individualized intelligence quotient and sub-domain scores. *Cerebral Cortex*, 30(3):888–900.

Kandanaarachchi, S. and Hyndman, R. J. (2021). Dimension reduction for outlier detection using dobin. *Journal of Computational and Graphical Statistics*, 30(1):204–219.

Kim, S.-J., Koh, K., Boyd, S., and Gorinevsky, D. (2009).  $\ell_1$  Trend Filtering. *SIAM Review*, 51(2):339–360.

Koo, T. K. and Li, M. Y. (2016). A Guideline of Selecting and Reporting Intraclass Correlation Coefficients for Reliability Research. *Journal of Chiropractic Medicine*, 15(2):155–163.

Le, T. H. and Hu, X. (1996). Retrospective estimation and correction of physiological artifacts in fMRI by direct extraction of physiological activity from MR data. *Magnetic Resonance in Medicine*, 35(3):290–298.

Lindquist, M. A. (2008). The Statistical Analysis of fMRI Data. *Statistical Science*, 23(4):439–464.

Lindquist, M. A., Geuter, S., Wager, T. D., and Caffo, B. S. (2019). Modular preprocessing pipelines can reintroduce artifacts into fMRI data. *Human Brain Mapping*, 40(8):2358–2376.

Liu, T. T. (2016). Noise contributions to the fMRI signal: An overview. *NeuroImage*, 143:141–151.

Liu, T. T., Naleci, A., and Falahpour, M. (2017). The Global Signal in fMRI: Nuisance or Information? *NeuroImage*, 150:213–229.

Marek, S., Tervo-Clemmens, B., Nielsen, A. N., Wheelock, M. D., Miller, R. L., Laumann, T. O., Earl, E., Foran, W. W., Cordova, M., Doyle, O., Perrone, A., Miranda-Dominguez, O., Feczko, E., Sturgeon, D., Graham, A., Hermosillo, R., Snider, K., Galassi, A., Nagel, B. J., Ewing, S. W., Eggebrecht, A. T., Garavan, H., Dale, A. M., Greene, D. J., Barch, D. M., Fair, D. A., Luna, B., and Dosenbach, N. U. (2019). Identifying reproducible individual differences in childhood functional brain networks: An ABCD study. *Developmental Cognitive Neuroscience*, 40:100706.

McKeown, M. J., Makeig, S., Brown, G. G., Jung, T.-P., Kindermann, S. S., Bell, A. J., and Sejnowski, T. J. (1998). Analysis of fmri data by blind separation into independent spatial components. *Human brain mapping*, 6(3):160–188.

Mejia, A. F., Nebel, M. B., Eloyan, A., Caffo, B., and Lindquist, M. A. (2017). PCA leverage: outlier detection for high-dimensional functional magnetic resonance imaging data. *Biostatistics (Oxford, England)*, 18(3):521–536.

Miller, K. L., Alfaro-Almagro, F., Bangerter, N. K., Thomas, D. L., Yacoub, E., Xu, J., Bartsch, A. J., Jbabdi, S., Sotiroopoulos, S. N., Andersson, J. L., et al. (2016). Multimodal population brain imaging in the uk biobank prospective epidemiological study. *Nature neuroscience*, 19(11):1523–1536.

Minka, T. P. (2000). Automatic choice of dimensionality for PCA. *M.I.T. Media Laboratory Perceptual Computing Section Technical Report*, 514:16.

Murphy, K., Birn, R. M., Handwerker, D. A., Jones, T. B., and Bandettini, P. A. (2009). The impact of global signal regression on resting state correlations: Are anti-correlated networks introduced? *NeuroImage*, 44(3):893–905.

Muschelli, J., Nebel, M. B., Caffo, B. S., Barber, A. D., Pekar, J. J., and Mostofsky, S. H. (2014). Reduction of motion-related artifacts in resting state fMRI using aCompCor. *NeuroImage*, 96:22–35.

Nielsen, A. N., Greene, D. J., Gratton, C., Dosenbach, N. U., Petersen, S. E., and Schlaggar, B. L. (2019). Evaluating the Prediction of Brain Maturity from Functional Connectivity after Motion Artifact Denoising. *Cerebral Cortex*, 29(6).

Parkes, L., Fulcher, B., Yücel, M., and Fornito, A. (2018a). An evaluation of the efficacy, reliability, and sensitivity of motion correction strategies for resting-state functional MRI. *NeuroImage*.

Parkes, L., Fulcher, B., Yücel, M., and Fornito, A. (2018b). An evaluation of the efficacy, reliability, and sensitivity of motion correction strategies for resting-state functional MRI. *NeuroImage*, 171:415–436.

Patel, A. X., Kundu, P., Rubinov, M., Jones, P. S., Vértes, P. E., Ersche, K. D., Suckling, J., and Bullmore, E. T. (2014). A wavelet method for modeling and despiking motion artifacts from resting-state fMRI time series. *NeuroImage*, 95:287–304.

Power, J. D., Barnes, K. A., Snyder, A. Z., Schlaggar, B. L., and Petersen, S. E. (2012). Spurious but systematic correlations in functional connectivity MRI networks arise from subject motion. *Neuroimage*, 59(3):2142–2154.

Power, J. D., Mitra, A., Laumann, T. O., Snyder, A. Z., Schlaggar, B. L., and Petersen, S. E. (2014). Methods to detect, characterize, and remove motion artifact in resting state fMRI. *NeuroImage*, 84.

Power, J. D., Plitt, M., Laumann, T. O., and Martin, A. (2017). Sources and implications of whole-brain fMRI signals in humans. *NeuroImage*, 146:609–625.

Pruim, R. H. R., Mennes, M., van Rooij, D., Llera, A., Buitelaar, J. K., and Beckmann, C. F. (2015). ICA-AROMA: A robust ICA-based strategy for removing motion artifacts from fMRI data. *NeuroImage*, 112:267–277.

Risk, B. B., Kociuba, M. C., and Rowe, D. B. (2018). Impacts of simultaneous multislice acquisition on sensitivity and specificity in fmri. *NeuroImage*, 172:538–553.

Risk, B. B., Murden, R. J., Wu, J., Nebel, M. B., Venkataraman, A., Zhang, Z., and Qiu, D. (2021). Which multiband factor should you choose for your resting-state fmri study? *NeuroImage*, 234:117965.

Rohe, K. and Zeng, M. (2020). Vintage factor analysis with varimax performs statistical inference. *arXiv preprint arXiv:2004.05387*.

Rosch, K. S., Mostofsky, S. H., and Nebel, M. B. (2018). ADHD-related sex differences in fronto-subcortical intrinsic functional connectivity and associations with delay discounting. *Journal of Neurodevelopmental Disorders*, 10(1).

Rousseeuw, P. J. and Van Zomeren, B. C. (1990). Unmasking multivariate outliers and leverage points. *Journal of the American Statistical association*, 85(411):633–639.

Salimi-Khorshidi, G., Douaud, G., Beckmann, C. F., Glasser, M. F., Griffanti, L., and Smith, S. M. (2014). Automatic denoising of functional MRI data: combining independent component analysis and hierarchical fusion of classifiers. *NeuroImage*, 90:449–468.

Satterthwaite, T. D., Ceric, R., Roalf, D. R., Davatzikos, C., Bassett, D. S., and Wolf, D. H. (2019). Motion artifact in studies of functional connectivity: Characteristics and mitigation strategies. *Human Brain Mapping*, 40(7):2033–2051.

Satterthwaite, T. D., Elliott, M. A., Gerraty, R. T., Ruparel, K., Loughead, J., Calkins, M. E., Eickhoff, S. B., Hakonarson, H., Gur, R. C., Gur, R. E., and Wolf, D. H. (2013a). An improved framework for confound regression and filtering for control of motion artifact in the preprocessing of resting-state functional connectivity data. *NeuroImage*, 64:240–256.

Satterthwaite, T. D., Wolf, D. H., Loughead, J., Ruparel, K., Elliott, M. A., Hakon, H., Gur, R. C., and Gur, R. E. (2012). Impact of In-Scanner Head Motion on Multiple Measures of Functional Connectivity: Relevance for Studies of Neurodevelopment in Youth. *NeuroImage*, 60(1):623–632.

Satterthwaite, T. D., Wolf, D. H., Roalf, D. R., Ruparel, K., Erus, G., Vandekar, S., Gennatas, E. D., Elliott, M. A., Smith, A., Hakonarson, H., Verma, R., Davatzikos, C., Gur, R. E., and Gur, R. C. (2015). Linked Sex Differences in Cognition and Functional Connectivity in Youth. *Cerebral Cortex*, 25(9).

Satterthwaite, T. D., Wolf, D. H., Ruparel, K., Erus, G., Elliott, M. A., Eickhoff, S. B., Gennatas, E. D., Jackson, C., Prabhakaran, K., Smith, A., et al. (2013b). Heterogeneous impact of motion on fundamental patterns of developmental changes in functional connectivity during youth. *Neuroimage*, 83:45–57.

Shehzad, Z., Kelly, A. C., Reiss, P. T., Gee, D. G., Gotimer, K., Uddin, L. Q., Lee, S. H., Margulies, D. S., Roy, A. K., Biswal, B. B., et al. (2009). The resting brain: unconstrained yet reliable. *Cerebral cortex*, 19(10):2209–2229.

Shirer, W. R., Jiang, H., Price, C. M., Ng, B., and Greicius, M. D. (2015). Optimization of rs-fMRI Pre-processing for Enhanced Signal-Noise Separation, Test-Retest Reliability, and Group Discrimination. *NeuroImage*, 117:67–79.

Shrout, P. E. and Fleiss, J. L. (1979). Intraclass correlations: uses in assessing rater reliability. *Psychological Bulletin*, 86(2):420–428.

Siegel, J. S., Mitra, A., Laumann, T. O., Seitzman, B. A., Raichle, M., Corbetta, M., and Snyder, A. Z. (2017). Data quality influences observed links between functional connectivity and behavior. *Cerebral Cortex*, 27(9):4492–4502.

Smyser, C. D., Inder, T. E., Shimony, J. S., Hill, J. E., Degnan, A. J., Snyder, A. Z., and Neil, J. J. (2010). Longitudinal Analysis of Neural Network Development in Preterm Infants. *Cerebral Cortex (New York, NY)*, 20(12):2852–2862.

Sobczyk, P., Bogdan, M., and Josse, J. (2017). Bayesian Dimensionality Reduction With PCA Using Penalized Semi-Integrated Likelihood. *Journal of Computational and Graphical Statistics*, 26(4):826–839.

Thomason, M. E., Dennis, E. L., Joshi, A. A., Joshi, S. H., Dinov, I. D., Chang, C., Henry, M. L., Johnson, R. F., Thompson, P. M., Toga, A. W., et al. (2011). Resting-state fmri can reliably map neural networks in children. *Neuroimage*, 55(1):165–175.

Tibshirani, R. (1996). Regression shrinkage and selection via the lasso. *Journal of the Royal Statistical Society. Series B (Statistical Methodology)*, 58(1):267–288.

Tibshirani, R. J. (2014). Adaptive piecewise polynomial estimation via trend filtering. *The Annals of Statistics*, 42(1):285–323.

Todd, N., Josephs, O., Zeidman, P., Flandin, G., Moeller, S., and Weiskopf, N. (2017). Functional sensitivity of 2d simultaneous multi-slice echo-planar imaging: effects of acceleration on g-factor and physiological noise. *Frontiers in Neuroscience*, 11:158.

Van Dijk, K. R. A., Sabuncu, M. R., and Buckner, R. L. (2012). The influence of head motion on intrinsic functional connectivity MRI. *NeuroImage*, 59(1):431–438.

Van Essen, D. C., Smith, S. M., Barch, D. M., Behrens, T. E. J., Yacoub, E., and Ugurbil, K. (2013). The WU-Minn Human Connectome Project: An overview. *NeuroImage*, 80:62–79.

Weintraub, S., Dikmen, S. S., Heaton, R. K., Tulsky, D. S., Zelazo, P. D., Bauer, P. J., Carlozzi, N. E., Slotkin, J., Blitz, D., Wallner-Allen, K., Fox, N. A., Beaumont, J. L., Mungas, D., Nowinski, C. J., Richler, J., Deocampo, J. A., Anderson, J. E., Manly, J. J., Borosh, B., Havlik, R., Conway, K., Edwards, E., Freund, L., King, J. W., Moy, C., Witt, E., and Gershon, R. C. (2013). Cognition assessment using the NIH Toolbox. *Neurology*, 80(11 Suppl 3).

Witten, D. M., Tibshirani, R., and Hastie, T. (2009). A penalized matrix decomposition, with applications to sparse principal components and canonical correlation analysis. *Biostatistics*, 10(3):515–534.

Yan, C.-G., Cheung, B., Kelly, C., Colcombe, S., Craddock, R. C., Di Martino, A., Li, Q., Zuo, X.-N., Castellanos, F. X., and Milham, M. P. (2013). A comprehensive assessment of regional variation in the impact of head micromovements on functional connectomics. *NeuroImage*, 76:183–201.

Yancey, S. E., Rotenberg, D. J., Tam, F., Chiew, M., Ranieri, S., Biswas, L., Anderson, K. J., Nicole Baker, S., Wright, G. A., and Graham, S. J. (2011). Spin-history artifact during functional MRI: Potential for adaptive correction. *Medical Physics*, 38(8):4634–4646.

Yeo, B. T. T., Krienen, F. M., Sepulcre, J., Sabuncu, M. R., Lashkari, D., Hollinshead, M., Roffman, J. L., Smoller, J. W., Zöllei, L., Polimeni, J. R., Fischl, B., Liu, H., and Buckner, R. L. (2011). The organization of the human cerebral cortex estimated by intrinsic functional connectivity. *Journal of Neurophysiology*, 106(3):1125–1165.

Zou, H. and Hastie, T. (2005). Regularization and variable selection via the elastic net. *Journal of the Royal Statistical Society: Series B (Statistical Methodology)*, 67(2):301–320.

Zuo, X.-N., Kelly, C., Adelstein, J. S., Klein, D. F., Castellanos, F. X., and Milham, M. P. (2010). Reliable intrinsic connectivity networks: test-retest evaluation using ica and dual regression approach. *Neuroimage*, 49(3):2163–2177.

## A FusedPCA

The original PCA leverage method (Mejia et al., 2017) calculates the scores by solving the following optimization problem

$$\begin{aligned} \min_{\mathbf{U}, \mathbf{V}} \quad & \frac{1}{2} \|\mathbf{X} - \mathbf{U}\Lambda\mathbf{V}^\top\|_F^2 \\ \text{subject to} \quad & \mathbf{U}^\top \mathbf{U} = \mathbf{I}_Q, \mathbf{V}^\top \mathbf{V} = \mathbf{I}_V. \end{aligned} \quad (1)$$

After calculating  $\mathbf{U}$ , the PCA leverage is given by the diagonal of  $\mathbf{U}\mathbf{U}^\top$ . When  $Q = 1$ , the optimization problem in Equation (1) is equivalent to

$$\begin{aligned} \max_{\mathbf{u}, \mathbf{v}} \quad & \mathbf{u}^\top \mathbf{X} \mathbf{v} \\ \text{subject to} \quad & \|\mathbf{u}\|_2^2 = 1, \|\mathbf{v}\|_2^2 = 1. \end{aligned} \quad (2)$$

If  $(\hat{\mathbf{u}}, \hat{\mathbf{v}}) = \text{argmax}_{\mathbf{u}, \mathbf{v}} \mathbf{u}^\top \mathbf{X} \mathbf{v}$  are such that  $\|\mathbf{u}\|_2, \|\mathbf{v}\|_2 \geq 1$ , then Equation (2) has a convex relaxation

$$\begin{aligned} \max_{\mathbf{u}, \mathbf{v}} \quad & \mathbf{u}^\top \mathbf{X} \mathbf{v} \\ \text{subject to} \quad & \|\mathbf{u}\|_2^2 \leq 1, \|\mathbf{v}\|_2^2 \leq 1. \end{aligned} \quad (3)$$

To enforce the desired piecewise-constant behavior for  $\mathbf{u}$ , FusedPCA modifies Equation (3) by adding a penalty for the first order differences, that is

$$\begin{aligned} \max_{\mathbf{u}, \mathbf{v}} \quad & \mathbf{u}^\top \mathbf{X} \mathbf{v} \\ \text{subject to} \quad & \|\mathbf{u}\|_2^2 \leq 1, \|\mathbf{D}\mathbf{u}\|_1 \leq c, \|\mathbf{v}\|_2^2 \leq 1, \end{aligned} \quad (4)$$

where  $c$  is a constant and  $\mathbf{D}$  is the first order difference operator

$$\mathbf{D} = \begin{pmatrix} 1 & -1 & & & \\ & 1 & -1 & & \\ & & \ddots & \ddots & \\ & & & 1 & -1 \end{pmatrix}. \quad (5)$$

By adding the first order difference penalty, the resulting  $\mathbf{u}$  will be piecewise constant when  $c$  is appropriately small. For computational purposes, we re-express the constraints on  $\mathbf{u}$  in Lagrange form

$$\begin{aligned} \min_{\mathbf{u}, \mathbf{v}} \quad & -\mathbf{u}^\top \mathbf{X} \mathbf{v} + \frac{1}{2} \mathbf{u}^\top \mathbf{u} + \kappa \|\mathbf{D}\mathbf{u}\|_1 \\ \text{subject to} \quad & \|\mathbf{v}\|_2^2 \leq 1. \end{aligned} \quad (6)$$

This problem is separately convex in  $\mathbf{u}$  and  $\mathbf{v}$ , and can be solved iteratively with  $\hat{\lambda}_1 = \max \mathbf{u}^\top \mathbf{X} \mathbf{v}$ . To extend to higher dimensions with  $Q > 1$ , we remove the part in  $\mathbf{X}$  that has already been explained by the previous  $k$  estimated components. Algorithm 1 makes this procedure explicit. After estimating the leverage scores, we use the same thresholding method to identify outliers as detailed above.

---

**Algorithm 1** FusedPCA

---

- 1: **Input:** centered and scaled  $\mathbf{X}$
- 2: Set  $\mathbf{X}^{(1)} = \mathbf{X}$
- 3: **for**  $k = 1, \dots, Q$  **do**
- 4:   Initialize  $\mathbf{v}_k$  as the first right singular vector of  $\mathbf{X}^{(k)}$
- 5:   Iterate until convergence:
- 6:     (1)  $\mathbf{u}_k \leftarrow \operatorname{argmin}_{\mathbf{u}} \frac{1}{2} \|\mathbf{u} - \mathbf{X}^{(k)} \mathbf{v}_k\|_2^2 + \kappa \|\mathbf{D}\mathbf{u}\|_1$
- 7:     (2)  $\mathbf{v}_k \leftarrow \frac{\mathbf{X}^{k\top} \mathbf{u}_k}{\|\mathbf{X}^{k\top} \mathbf{u}_k\|_2}$
- 8:      $\lambda_k \leftarrow \mathbf{u}_k^\top \mathbf{X}^k \mathbf{v}_k$
- 9:      $\mathbf{X}^{k+1} = \mathbf{X}^k - \lambda_k \mathbf{u}_k \mathbf{v}_k$
- 10: **end for**
- 11: **Return:** the scores  $\mathbf{u}_k$  for  $k = 1, \dots, Q$

---

## B Kurtosis-based selection of artifactual directions

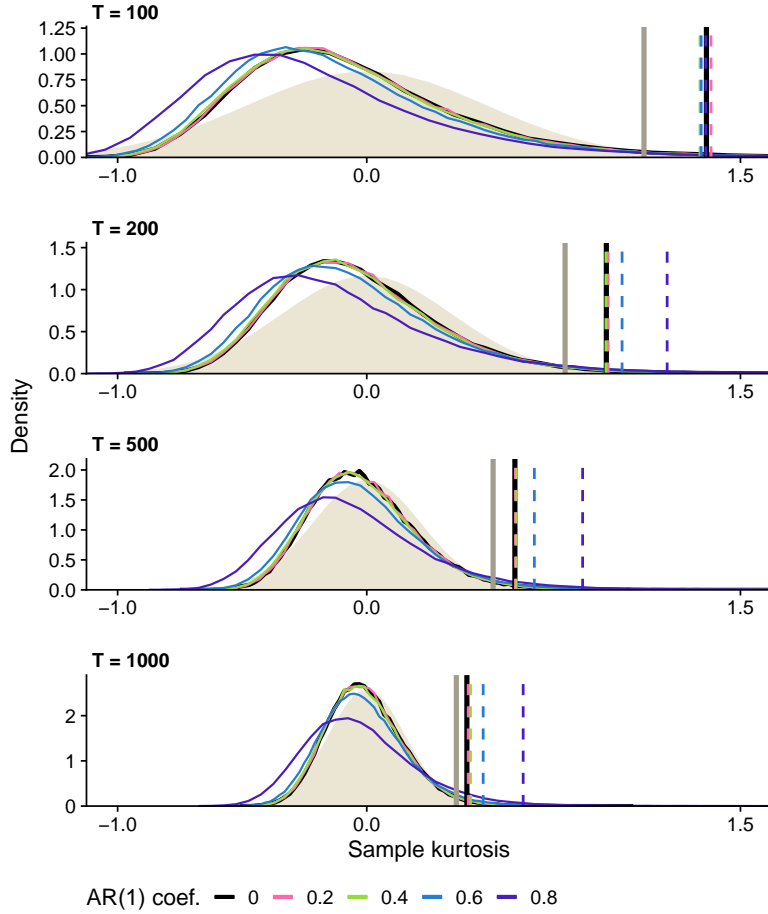


**Figure B.1: Effect of sample size and autocorrelation on the sampling distribution of kurtosis in normally distributed data with no outliers.** Each density curve is based on 100,000 Monte Carlo samples of a given sample size and autocorrelation level. The theoretical asymptotic distribution of kurtosis for non-autocorrelated data at each sample size is shown in light brown (Fisher, 1930). Vertical lines indicate each distribution's 0.99 quantile, the threshold used to identify component timeseries likely to contain outliers. For smaller sample size, the sampling distribution of kurtosis is right-skewed, becoming more symmetric and converging to a normal distribution as sample size increases. For sample size below 1000, the asymptotic distribution is not appropriate. Therefore, for scan duration  $T < 1000$  we use simulation to determine the 0.99 quantile; for longer durations, we use the theoretical 0.99 quantile based on the asymptotic distribution. The presence of weak to moderate autocorrelation (e.g. AR(1) coefficient  $\phi \leq 0.6$ ) has little effect on the sampling distribution of kurtosis.

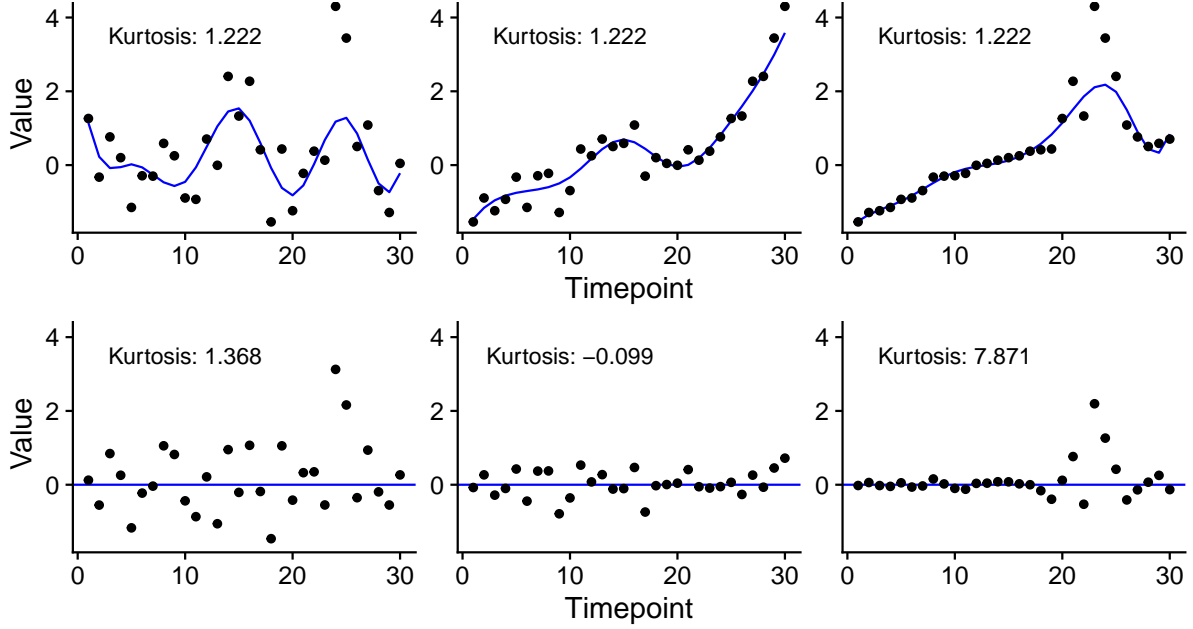


**Figure B.2: Effects of timeseries trends on kurtosis.** The presence of trends can invalidate kurtosis as a measure of outlier presence. In the top panel, all three timeseries have the same kurtosis value of 1.222, below the high-kurtosis threshold. The first has a weak trend but no outliers, the second has a strong trend, and the third has both a trend and outliers. The bottom panel shows the same timeseries after detrending. Detrending has little effect on the kurtosis of the first timeseries, decreases the kurtosis of the second timeseries, and strongly increases kurtosis for the third dataset (the only one containing outliers). This illustrates the importance of detrending before using kurtosis to detect the presence of outliers.

## C Cross-validation procedure

We divided subjects into eight folds of approximately 100 subjects per fold by randomly assigning subjects in each sex and age group into each fold, so that each fold had an approximately equal number of males and females and a similar age distribution as the full sample. All four scans for each subject were assigned to the same fold.

For each of the eight test folds, the other seven folds were used as the training set for parameter and coefficient estimation. To choose the tuning parameters (the shrinkage penalty parameter  $\lambda$  and, in the case of sex prediction, the elastic net weight parameter  $\alpha$ ), cross-validation (CV) was used across the seven training folds. Specifically, 100  $\lambda$  values were considered for each of five values of  $\alpha \in \{0, .25, .5, .75, \text{ or } 1\}$ . For each  $\alpha$ , the “1se” rule was used to choose lambda, and then the  $\alpha$  with the lowest CV error was chosen. The regression coefficients were then estimated based on the model fit on all seven training folds, given the chosen tuning parameter(s), and was then applied to predict the scans in the

test fold.

In all models, the predictors are the Fisher  $z$ -transformed FC values, which are scaled for the training and test sets separately for each fold. Total cognition was centered and scaled within the test and training sets for each fold. The model for total cognition did not include an intercept since the predictors and outcome were both centered.

## D Alternative baselines

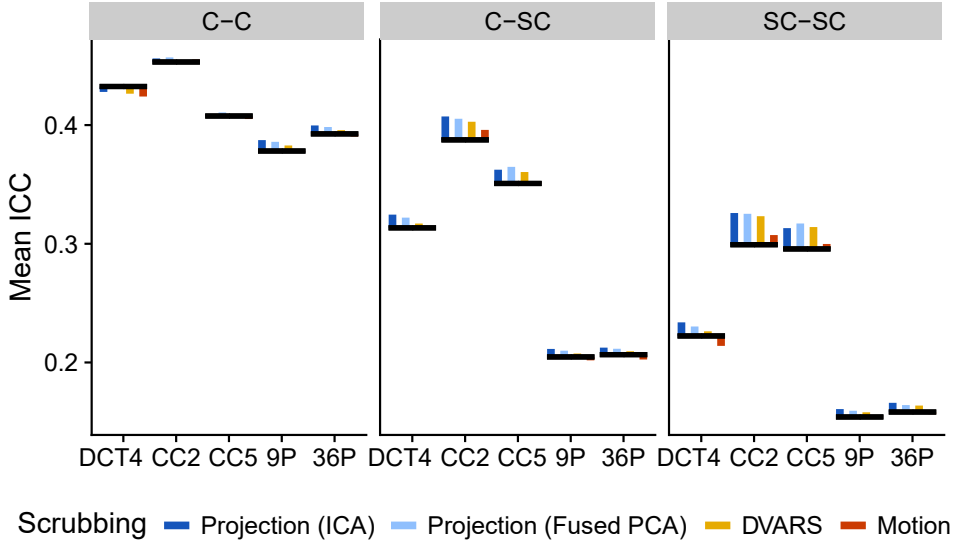


**Figure D.3: FC reliability improvement with scrubbing using different baselines.** We estimate FC after applying five different denoising strategies: detrending only (DCT4), CompCor with two components (CC2), CompCor with five components (CC5), the 9 parameter model (9P), and the 36 parameter model (36P). (All denoising strategies are regression-based, and each includes four DCT bases for detrending.) The ICCs of the FC estimates are calculated and averaged after grouping by connection type: intra-cortical (C-C), cortex-subcortex (C-SC), or intra-subcortical (SC-SC). The averages for each denoising method and connection type are indicated by black horizontal lines. Then, FC estimation is repeated while combining each scrubbing method with each denoising method. (We use the same cutoffs as in our primary analysis: 3 times the median for projection scrubbing, the dual cutoff for DVARS, and 0.3 mm for FD.) The colored vertical lines indicate the change in mean ICC attributable to scrubbing by connecting the mean ICC with scrubbing to the mean ICC without scrubbing, for each baseline and connection type. For example, colored lines that extend upward from a black line indicate an improvement to FC reliability from the respective baseline.

In our primary analysis we compared scrubbing methods using CompCor with two components (CC2) as our baseline. CC2 was selected because it yielded the highest mean ICC. However, the other denoising strategies we considered are also commonly used for fMRI data cleaning. In Figure D.3, we explore the improvement in reliability of FC estimates using scrubbing in addition to a few of these other baselines. Across the different baselines, scrubbing tends to improve reliability, especially for subcortical connections, but those subcortical improvements are smaller for the 9P and 36P baselines. Between the different scrubbing methods, projection scrubbing and DVARS tend to outperform motion scrubbing, and projection scrubbing performs slightly better than DVARS overall. This generalizes our findings, which suggest that motion scrubbing is less effective than data-drive scrubbing methods, and projection

scrubbing tends to produce the most reliable FC estimates.